

Review

Cancer Stratification by Molecular Imaging

Justus Weber, Uwe Haberkorn and Walter Mier *

Heidelberg University Hospital, Department of Nuclear Medicine, Im Neuenheimer Feld 400, 69120 Heidelberg, Germany; E-Mails: ju.weber.ma@gmx.de (J.W.); uwe.haberkorn@med.uni-heidelberg.de (U.H.)

* Author to whom correspondence should be addressed; E-Mail: walter.mier@med.uni-heidelberg.de; Tel.: +49-6221-567720; Fax: +49-6221-565473.

Academic Editor: William Chi-Shing Cho

Received: 15 October 2014 / Accepted: 17 February 2015 / Published: 4 March 2015

Abstract: The lack of specificity of traditional cytotoxic drugs has triggered the development of anticancer agents that selectively address specific molecular targets. An intrinsic property of these specialized drugs is their limited applicability for specific patient subgroups. Consequently, the generation of information about tumor characteristics is the key to exploit the potential of these drugs. Currently, cancer stratification relies on three approaches: Gene expression analysis and cancer proteomics, immunohistochemistry and molecular imaging. In order to enable the precise localization of functionally expressed targets, molecular imaging combines highly selective biomarkers and intense signal sources. Thus, cancer stratification and localization are performed simultaneously. Many cancer types are characterized by altered receptor expression, such as somatostatin receptors, folate receptors or Her2 (human epidermal growth factor receptor 2). Similar correlations are also known for a multitude of transporters, such as glucose transporters, amino acid transporters or hNIS (human sodium iodide symporter), as well as cell specific proteins, such as the prostate specific membrane antigen, integrins, and CD20. This review provides a comprehensive description of the methods, targets and agents used in molecular imaging, to outline their application for cancer stratification. Emphasis is placed on radiotracers which are used to identify altered expression patterns of cancer associated markers.

Keywords: cancer stratification; molecular imaging; radiotracers; positron emission tomography (PET); single photon emission computed tomography (SPECT); biomarkers; target structure

1. Introduction

Stratified medicine deploys highly specific drugs for treatment purposes. By virtue of their specificity, these drugs are only applicable in subgroups of patient collectives, which show expression of the required target structure or target isoform. In order to provide patients with the most effective treatment as quickly as possible, clustering of patient subgroups according to target expression patterns is of utmost importance (see Figure 1). The most important methods in the area of patient stratification are cancer proteomics, immunohistochemistry and molecular imaging [1]. Cancer proteomics mainly relies on monitoring serum biomarkers for diagnostic, prognostic or stratification purposes [2] and plays an important role in the discovery of signaling pathways [3] and gene expression profiling [4], which altogether can be used for cancer stratification. The emphasis of cancer proteomics is placed on functional analysis of deregulated cellular pathways and their role in the pathogenesis of a disease [5].

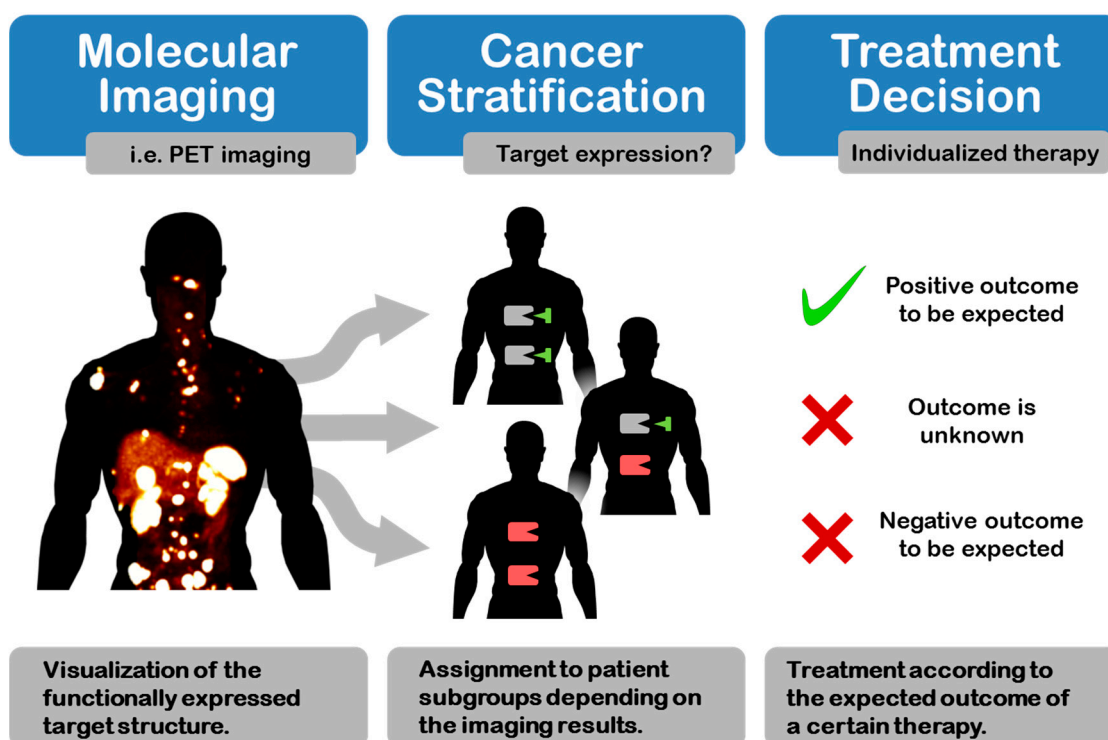


Figure 1. Cancer stratification by molecular imaging allows patients clustering according to the expected outcome of a therapeutic approach by visualizing an expressed biomarker. The resulting patient subgroups can subsequently be treated with the most promising therapy [6].

Molecular imaging describes *in vivo* imaging methods that use selective biomarkers in order to gain functional and anatomical information about the patient. For this purpose, many different imaging techniques are currently in use, the most prominent being positron emission tomography (PET) and single photon emission computed tomography (SPECT) [7]. Other important medical imaging methods, such as computed tomography (CT) and magnetic resonance imaging (MRI) require high amounts of contrast agents in order to derive functional information. This limits their applicability for molecular imaging; so far CT and MRI have not been implemented in the clinical molecular imaging routine [8,9].

The basic strategy of molecular imaging is the combination of highly selective biomarkers and efficient signal sources. Especially the use of radioactive substances by PET and SPECT is of particular interest in the field of oncology. This is mainly due to the low detection limit of radioactive decays, which allows functional imaging at high resolution with minimal tracer quantities, compared to CT or MRI [6,7]. Molecular imaging shows several advantages over other stratification methods: It is non-invasive and allows simultaneous, real-time and *in vivo* cancer detection and localization by visually proving the presence of an expressed biomarker both in the primary tumor and in metastases throughout the body. As molecular imaging relies on highly affine tracer molecules, this also provides an approach for targeted cancer therapy: Substitution of the diagnostic signal source by a cytotoxic moiety results in a therapeutic compound [8].

2. Targets for Cancer Stratification by Molecular Imaging

2.1. Glucose Utilization

The cellular uptake of glucose is mediated by two distinct types of transporters: sodium-dependent glucose transporters (SGLT) and glucose transporters (GLUT). So far, 12 members of the SGLT family are known. They belong to the solute carrier 5 family (SLC5) and function as sodium/glucose symporters [10]. GLUTs, on the other hand, belong to the solute carrier 2 family (SLC2) and allow facilitated diffusion of glucose along its concentration gradient. At present, 14 members of the GLUT family are known [11]. They have been clustered in three different groups depending on sequence homologies [12].

In the absence of sufficient amounts of oxygen, the cellular glucose metabolism changes and glucose is no longer fully oxidized. Under anaerobic conditions, cells rely more or less exclusively on glycolysis for the generation of energy and on the production of lactate, in order to regenerate the amount of NAD⁺ consumed during glycolysis [13,14]. In order to generate the energy required, cells increase their glucose uptake. There are many organs which are known for their high glucose uptake, such as heart, liver and brain. In addition, inflammations also show high glucose uptake [15,16].

The metabolism of cancer cells differs highly from that of normal cells of the same tissue: Many cancer types show increased glucose uptake and utilization, even under non-hypoxic conditions [11,17]. Depending on the type of cancer observed, glucose uptake can be increased by about 20- to 30-fold when compared to normal tissue and glycolysis was also shown to be performed up to 30-times quicker in cancer cells [18]. Yet, increased glucose uptake is also seen under non-hypoxic conditions in cancer tissue [17]. Nonetheless, hypoxia in cancer correlates with parameters of increased cancer aggressiveness, such as chemotherapy resistance [19] and an increased risk for the formation of metastasis [20]. Recently, it could be shown that the reliance on glycolysis has several advantages for cancer cells. First of all, it allows the generation of side products by removing intermediates from the citric cycle [21]. Secondly, the production of lactate itself provides a powerful tool for cancer cells: The secretion of lactate to the surrounding tissue leads to an acidification, to which most host cells cannot adapt and therefore die [22,23]. Additionally, an angiogenic effect of lactate has been shown recently [24]. Many cancer types show an overexpression of GLUT1 [25]. This observation correlates with many parameters employed to determine cancer aggressiveness, such as high potential to invade surrounding tissues, high risk for the generation of metastasis and chemotherapy resistance [26,27].

2-Deoxy-2-(^{18}F)fluoro-glucose (^{18}F -FDG; see Figure 2) is one of the most well-known agents for molecular imaging. Because of its structural and chemical properties, it is taken up like unmodified glucose and is phosphorylated by hexokinase subsequently, leading to intracellular retention. However, it is not further metabolized afterwards due to the missing 2-hydroxyl-group [28]. Since glucose-6-phosphate and structural derivatives, such as 2-deoxy-2-(^{18}F)fluoro-glucose-6-phosphate, have no GLUT substrate anymore, this leads to a tracer accumulation in tissues with high glucose uptake, such as cancer tissues, brain and liver [29]. This accumulation is also due to the differential regulation of other proteins of the glucose metabolism, such as a down-regulation of glucose-6-phosphatase [30] and increased glucose uptake triggered by the overall up-regulation of downstream glycolytic enzymes [31]. These effects lead to increased glucose uptake and FDG accumulation in tissues with high enzymatic activity. FDG-PET imaging subsequently allows the detection of tissues showing high glucose accumulation, by monitoring the incorporated β^+ emitting ^{18}F .



Figure 2. Chemical structure of 2-Deoxy-2-(^{18}F)fluoro-glucose (^{18}F -FDG). ^{18}F -FDG is taken up by the glucose transport system. As many cancer types show higher metabolic glucose turnover, ^{18}F -FDG uptake is increased, leading to its accumulation in cancer tissue. Subsequently, imaging with positron emission tomography (PET) is possible due to the β^+ emitting radionuclide ^{18}F .

^{18}F -FDG-PET has been successfully used for detection and tumor staging of different cancer types over the last 20 years, such as lung cancer [32], breast cancer [33], renal cell carcinomas [34] and many others, as reviewed by Gallamini *et al.* [35] and Hawkins *et al.* [36].

2.2. Amino Acid Utilization

Due to their charge, amino acids are unable to permeate cell membranes. The carriers responsible for amino acid uptake belong to the solute carrier families SLC3 and SLC7 [37]. SLC7 carriers can be divided into two groups: cationic amino acid transporter (CAT) and L-type amino acid transporters (LAT). CATs perform sodium independent L-type amino acid uptake by facilitated diffusion [38–40]. LATs, on the other hand, mainly work as amino acid antiporters, by exporting non-essential amino acids in exchange for essential amino acids [37,41,42].

LATs always occur as heterodimers with members of the SLC3 family. The heterodimeric construct is then called HAT (heterodimeric amino acid transporter). There are only two known members of the SLC3 family: 4F2hc and rBAT, which belong to the group of type II transmembrane *N*-glycoproteins [43]. The SLC3 members are responsible for the cellular trafficking of the receptor towards the plasma membrane [44]. The substrate specificity of HATs mainly depends on the LAT incorporated in the heterodimer [37].

4F2hc/LAT1(L-type amino acid transporter 1) is overexpressed in many kinds of tumors, such as cervical carcinoma [45], gastric carcinoma [46] and different forms of leukemia—to name only

a few [41,47]. High LAT1 expression is associated with parameters of high cancer aggressiveness, such as lymph node metastasis and angiogenesis [48,49]. Another amino acid transporter that is often overexpressed in cancer is ASCT2 (ASC amino-acid transporter 2), which is responsible for the sodium dependent uptake of neutral amino acids [50,51]. It is overexpressed in prostate cancer and hepatocellular cancer and is also associated with high cancer aggressiveness [52].

Similar to the imaging with [^{18}F]-FDG, radiolabeled amino acids can be used to image tissues with increased amino acid throughput. This is especially the case for cancer cells, which usually replicate very quickly and therefore require higher amount of amino acids [51].

The main application of amino acid radiotracers is the detection of tumors characterized by varying glucose uptake, which makes them impossible to monitor reliably and reproducibly with [^{18}F]-FDG. One such example is neuroendocrine tumors [53,54].

As amino acid transporters are ubiquitously expressed, a high selectivity of the tracer molecule is of major importance. In the last years a huge amount of amino acid radiotracers has been developed for PET or SPECT [55]. Here, we only focus on a few selected tracer molecules.

A few years ago, it could be shown that the SPECT tracer L-3- ^{123}I -iodo- α -methyl-tyrosine shows high LAT1 specificity, compared to other uptake mechanisms [56]. The major disadvantage of this tracer is that it has to be monitored with SPECT, which has a significantly lower resolution than PET. Thus, ^{18}F -labeled compounds, such as L-3- ^{18}F - α -methyl-tyrosine ([^{18}F]-FAMT) have been developed (see Figure 3), in order to benefit from the high PET resolution [57]. This development only became possible upon the discovery that the α -methyl group is responsible for LAT1 specificity [58]. [^{18}F]-FAMT is currently one of the most specific and most often used PET tracers for the imaging of cancers with low glucose uptake rates [59,60].

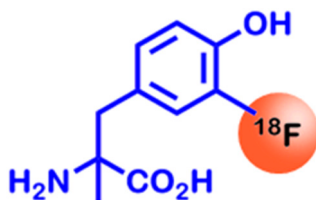


Figure 3. Chemical structure of L-3- ^{18}F - α -methyl-tyrosine, a PET tracer specifically taken up via amino acid transporters, which are overexpressed in many types of cancer.

2.3. Somatostatin Receptors

Somatostatin receptors (SSTRs) play an important role in the inhibition of growth hormone secretion [61], as well as the production and secretion of gastrointestinal hormones, such as gastrin, renin, glucagon and insulin [62]. SSTRs are known to internalize upon ligand binding [63]. The ligand, somatostatin, is a peptide hormone that is secreted by different tissues of the gastrointestinal tract and stomach. Somatostatin is activated by protease cleavage and occurs in two versions—somatostatin-14 and somatostatin-28 [64].

SSTR2 is the most abundant receptor isoform and is overexpressed in many tumors; especially in neuroendocrine tumors [65]. Additionally, it shows the highest SSTR internalization rate, which makes it a valuable target for molecular imaging and targeted therapy [63,66]. As somatostatin has a short

biological half-life (about 3 min) [67], more stable synthetic versions have been developed for clinical applications [64,68]. In 1978, Vale *et al.* published a comparative analysis of a series of somatostatin analogues, which have been improved further since then [69]. Currently, octreotide is one of the most often used somatostatin analogues. It shows high binding affinity to SSTR2 [65] and exhibits a 19-fold stronger inhibitory effect on the growth hormone secretion than native somatostatin [70].

One of the most well-known octreotide derivatives for therapeutic and imaging purposes is DOTATOC (DOTA(0)-Phe(1)-Tyr(3))octreotide) (see Figure 4). Chemically, it consists of the chelator DOTA (1,4,7,10-tetraazacyclododecane-1,4,7,10-tetraacetic acid) which is linked to octreotide via a peptide bond. The octreotide employed was further modified by substituting phenylalanine at position three with tyrosine, in order to increase the stability of the compound [71]. DOTA is able to chelate many different radionuclides, such as ^{68}Ga , ^{111}In or ^{90}Y . While ^{68}Ga and ^{111}In are used for molecular imaging and cancer stratification via PET and SPECT, ^{90}Y can be used to subsequently treat patients with SSTR-overexpressing cancers [72].

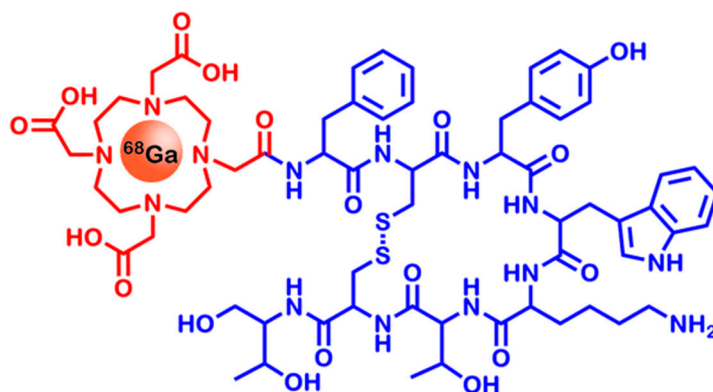


Figure 4. Chemical structure of [^{68}Ga]-DOTATOC (DOTA(0)-Phe(1)-Tyr(3))octreotide). It shows high affinity to SSTR2 (Somatostatin Receptor 2)—a receptor overexpressed in neuroendocrine tumors. The blue portion of the molecule is responsible for the SSTR2 specificity, whereas the radionuclide ^{68}Ga contained in the chelator DOTA (red) acts as the signal source for PET imaging. For reasons of clarity, chelation bonds are omitted.

In a comparative study, it could be shown recently that the radionuclide incorporated in the tracer has a considerable influence on the target specificity. Gallium chelated octreotide derivatives showed an increased SSTR2 specificity by up to factor five, when compared to the same tracer carrying ^{111}In . Additionally the tumor uptake was 2.5-times higher for gallium carrying tracer molecules. Kidney uptake was also shown to be decreased compared to ^{111}In -octreotide tracers [73,74].

Recently, a next-generation somatostatin analogue (SOM230, Signifor[®], Novartis, Switzerland) has been developed for therapeutic purposes. Signifor[®] was granted an orphan drug status for therapy of the Cushing's disease by both EMA in 2009 and FDA in 2012. SOM230 distinguishes from its predecessors through its high affinity to all five SSTRs. Moreover, its potency is 3- to 4-fold higher than that of octreotide and elimination from the circulation is prolonged about 10-times to a physical half-life of 23 h [75]. So far, SOM230 is not used as a radiotracer for molecular imaging. Nonetheless, this application could play an important role in the future, due to the high importance of octreotide

based tracers for the clinical molecular imaging routine and the improved performance of SOM230 as compared to other SSTR-tracers.

2.4. Integrins

Integrins are a family of heterodimeric receptors and play an important role in cell adhesion and cell signaling. So far, 19 α - and 8 β -integrin-subunits are known, which occur in 24 different arrangements in most vertebrates [76,77]. Receptor specificity mainly depends upon the α -subunit incorporated in the receptor [78]. The 24 members of the vertebrate integrin family are able to interact with several different molecules, such as collagen, laminin and RGD-motif (Arg-Gly-Asp) containing molecules, e.g., fibronectin and vitronectin [79]. Upon ligand binding, integrins induce different intracellular signaling pathways [80]. They play an important role in a multitude of processes that are crucial for tumor progression such as up-regulation and recruitment of tissue-metalloproteases, migration and angiogenesis [81,82]. The most common and well-studied integrins playing an important role in cancer, especially in promoting angiogenesis, are those containing an α_v -subunit. [83]. Overexpression of integrin $\alpha_v\beta_3$ is most often seen in glioblastomas and melanomas [84,85]. Since the α -subunit mainly determines the receptor specificity, most α_v containing integrins can be targeted with similar tracers containing an RGD-motif.

The first linear RGD-tracers were developed in 2001 [86] and later on modified by developing more stable cyclic RGD-tracers. In order to decrease protease digestibility of the compound, D-amino acids have been incorporated. There are numerous different RGD-tracers nowadays, as reviewed by Cai *et al.* [87]. Cyclic RGDfV (Cyclo [Arg-Gly-Asp-D-Phe-Val]) is the most prominent lead structure to target integrin $\alpha_v\beta_3$ [88,89]. In order to generate a theranostic compound, radiolabeling with both diagnostic and therapeutic radionuclides has to be possible. For this purpose, coupling of chelators is very useful, because they allow quick and variable radionuclide usage (see Figure 5).

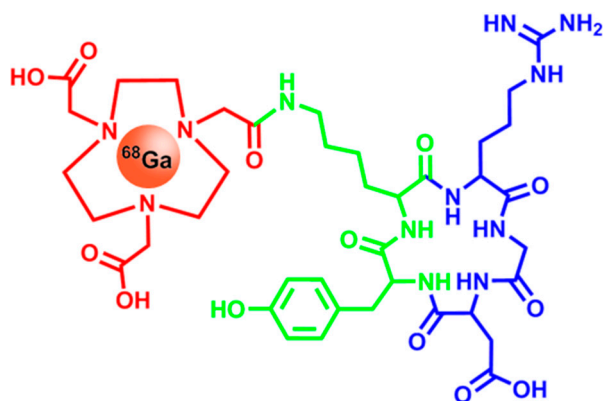


Figure 5. Chemical structure of [^{68}Ga]-NOTA-c(RGDyK) (NOTA-Cyclo [Arg-Gly-Asp-D-Tyr-Lys]), which is used for the molecular imaging of $\alpha_v\beta_3$ integrin overexpressing tumors. ^{68}Ga functions as the signal source for molecular imaging and is chelated to NOTA (red) to prevent displacement of the imaging moiety. The RGD-motif (Arg-Gly-Asp, blue) is responsible for the integrin interaction. Insertion of D-tyrosine and cyclization reduce the protease digestibility of the compound, while lysine enables the correct positioning of the imaging moiety. For reasons of clarity, chelation bonds are omitted.

Recently, it was observed that Ga^{3+} ions are too small to perfectly fit into DOTA [90]. Additionally, DOTA-conjugated RGD-tracers showed high blood pool activity due to unspecific interactions with plasma proteins. Thus, smaller chelators, such as NOTA (1,4,7-triazacyclononane-triacetic acid) became more important. However, coupling of chelators to c(RGDfV) was not possible, because all chemically addressable groups could not be modified without influencing the pharmacophore. For this reason, valine was substituted by lysine in order to incorporate an addressable amino functionality. Additional modifications, such as other D-amino acids, were mainly introduced in order to influence pharmacokinetic parameters and increase the serum stability by preventing protease cleavage [89,91]. NOTA-c(RGDyK) showed high integrin $\alpha_v\beta_3$ affinity ($K_i = 3.6$ nM) and decreased blood pool activity [92].

2.5. Folate Receptors

Folic acid (pteroylmono-glutamic acid) plays an important role in the biosynthesis of amino acids, purines and thymidylates by acting as a C1-group donor [93]. Mammals are unable to synthesize folate and therefore rely on their diet to keep their folate levels constant [94].

So far, three different folate uptake mechanisms are known: reduced folate carriers, proton coupled folate transporters and folate receptors (FR). Reduced folate carriers are bidirectional antiporters that import folate in exchange for negatively charged biomolecules, such as adenosine phosphates [95]. Proton coupled folate transporters, on the other hand, are proton/folate symporters that deploy energy derived from the transmembrane proton gradient to import folate against its concentration gradient into the cell [96]. Both of the previously mentioned transport mechanisms show low folate binding affinity in comparison to the FR ($K_D \approx 10^{-10}$ M) [97]. The FR exists in three different isoforms (FR α , FR β and FR γ) and leads to folate internalization by receptor mediated endocytosis [98]. FR overexpression has been detected in different tumor entities, mainly arising from epithelial tissue, as summarized in Table 1. Additionally FR overexpression correlates with poor prognosis, due to high cancer aggressiveness and chemotherapy resistance [99].

Table 1. Folate receptor overexpression in different cancer types [100]. FR, folate receptors.

Cancer Type	Rate of FR Overexpression
Ovarian	93%
Endometrial	90%
Renal	50%
Lung	33%
Colorectal	22%
Breast	21%

One of the most promising approaches in targeting FR overexpressing tumors is the utilization of folate derivatives, which feature high binding affinities and clear, thus patentable, structures [101]. Vintafolide/etarfolatide, two compounds developed by Endocyte Inc. (West Lafayette, IN, USA) and Merck & Co (Kenilworth, NJ, USA), provide an example for this group of compounds. As shown in Figure 6, both compounds consist of folic acid, which is responsible for the targeting, and either a diagnostic or a therapeutic moiety. The therapeutic component, vintafolide, contains a hydrophilic peptide spacer, a cleavable disulfide-linker and the therapeutic agent deacetylvinblastine monohydrate, which is a

microtubule inhibiting agent [102]. Etarfolatide, on the other hand, contains a non-cleavable peptide bond to prevent displacement of the chelator together with the imaging compound ^{99m}Tc [103–105]. Early clinical trials proved good results for vintafolide and etarfolatide, however, both compounds have been withdrawn from the European market for the indication of “FR-positive, platinum-resistant ovarian cancer in adult women”, since no significant improvement compared to the current therapy could be shown. Nonetheless, vintafolide is still in clinical trials for its application in “FR-positive, recurrent non-small cellular lung carcinoma”. Most recently, it could be shown that combination therapy with docetaxel leads to increased overall survival rates [106].

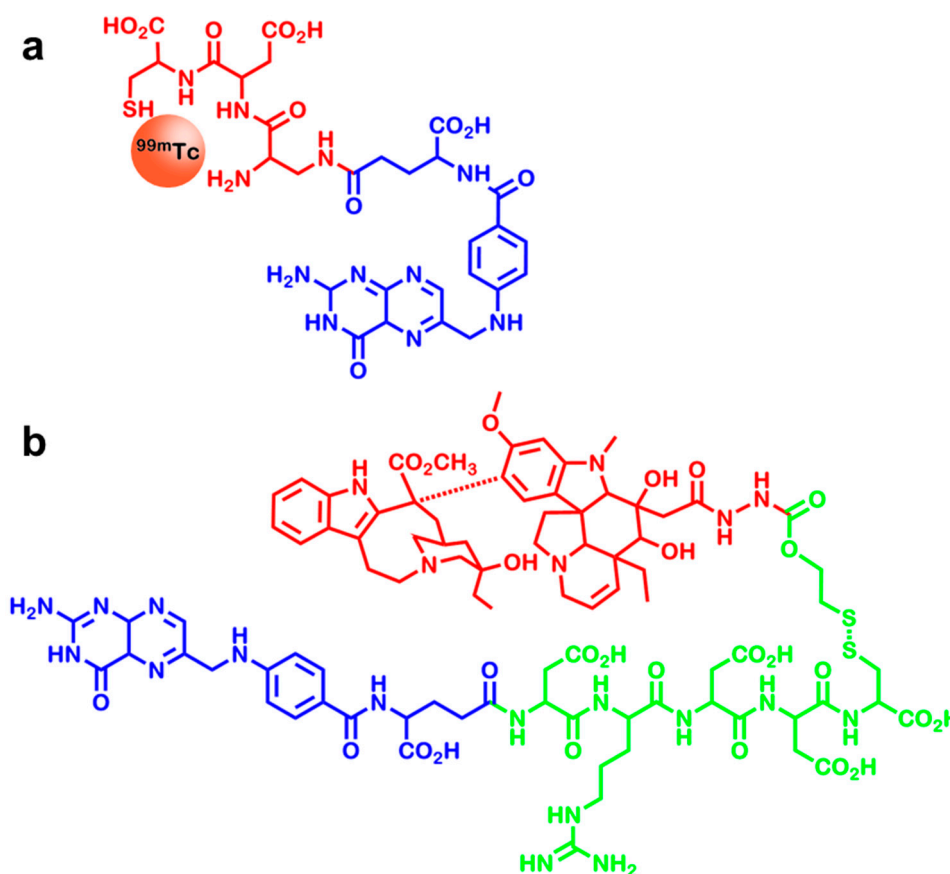


Figure 6. (a) Chemical structure of etarfolatide. It is used to image folate receptor positive cancers with SPECT. It contains folate (blue) to target the compound to the FR and chelated ^{99m}Tc in order to allow imaging (red); (b) Chemical structure of vintafolide, which is used to treat folate receptor positive ovarian cancer. It also contains folate as targeting moiety (blue). Additionally, a hydrophilic peptide linker with a cleavable disulfide bond (green) is incorporated to allow the release of deacetylvinblastine monohydrazide (red), which exhibits the cytotoxic effect. For reasons of clarity, chelation bonds are omitted.

2.6. CD20

CD20 is an integral membrane protein exclusively expressed on B cells, with the exception of fully differentiated plasma cells, and may thus be used as a B-cell marker [107,108]. It plays an important role in B-cell differentiation and activation [109], cell cycle progression [110] and Ca^{2+} uptake [111,112].

Additionally, CD20 is significantly involved in altering gene expression patterns [113] by activating down-stream signaling cascades, such as the c-Myc pathway [114].

The natural ligand of CD20 is not known so far [115,116]. CD20 is expressed on the surface of most malignant B-cells, even though expression levels may vary significantly [108]. Aggressive B-cell lymphomas very often show high expression levels, correlating with the cancer associated tissue dedifferentiation, which leads to CD20 up-regulation [117].

Zevalin[®] (ibritumomab-tiuxetan, Bayer Healthcare, Leverkusen, Germany) is a monoclonal anti-human-CD20 antibody that is covalently coupled to the chelator molecule tiuxetan (see Figure 7). In combination with the radionuclides ⁹⁰Y (therapeutic nuclide) and ¹¹¹In (diagnostic nuclide) it is approved for the treatment of “relapsed or refractory low-grade, follicular or transformed B-cell non-Hodgkin’s lymphoma”.

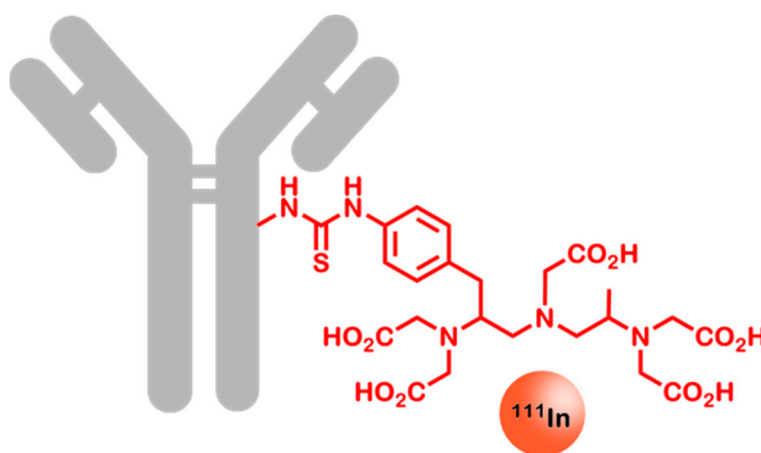


Figure 7. ¹¹¹In-ibritumomab-tiuxetan (Zevalin[®]). The monoclonal antibody ibritumomab (grey) is highly specific for CD20, which is overexpressed by many different lymphomas. The chelator tiuxetan (red) is able to bind ¹¹¹In, as well as ⁹⁰Y. This allows molecular imaging and the subsequent therapy of CD20 positive lymphomas. For reasons of clarity, chelation bonds are omitted.

In the US, molecular imaging using SPECT with ¹¹¹In-ibritumomab-tiuxetan is mandatory in order to verify the presence of CD20 prior to applying the therapeutic antibody. Additionally, correct biodistribution of the therapeutic compound can be confirmed by post-therapeutic imaging [118].

After having blocked CD20 on non-cancerous B-cells using 250 mg/m² unlabeled rituximab, 185 MBq of ¹¹¹In-Zevalin[®] is applied four hours later, followed by subsequent SPECT imaging.

In a comparative study the overall response rate (ORR) of therapeutic Zevalin[®] was 80% while the non-radiolabeled Rituximab only showed an ORR of 56%. The total time to progression was greater than 12 months in 37% of patients treated with Zevalin[®] [119,120]. It is very likely that this increase is, at least in part, also due to the previous cancer stratification by molecular imaging. Thus, only patients with an expected positive outcome are treated.

2.7. Her2

Her2 (human epidermal growth factor receptor 2) is a transmembrane glycoprotein belonging to the epidermal growth factor receptor family [121]. Members of this family are receptor tyrosine kinases: receptor dimers are formed upon ligand binding, which induces intracellular tyrosine side chain phosphorylation and leads to downstream signaling. Epidermal growth factor receptors play an important role in cell growth, cell differentiation and cell survival [122].

In contrast to other epidermal growth factor receptors, Her2 is constitutively activated and thus leads to permanent intracellular signaling. Her2 is overexpressed in many different cancer types, such as gastric cancer, ovarian cancer or non-small-cellular lung carcinomas [123]. It is also overexpressed in a significant portion (about 20%) of breast cancers. Her2 overexpression is associated with increased cell proliferation rates and chemotherapy resistance [124].

Her2 positive breast cancer is commonly treated by administration of the monoclonal antibody trastuzumab (Herceptin[®], Genentech, San Francisco, CA, USA) or the antibody-drug-conjugate ado-trastuzumab emtansine (Kadcyla[®], Roche, Basel, Switzerland) [125]. Ado-trastuzumab emtansine contains on average 3.5 covalently coupled DM1 molecules per antibody. DM1 induces cell death by tubuline inhibition [126].

In order to ensure a therapeutic effect, tumor staging is inevitable. Currently, radiotracers for *in vivo* imaging are being developed, in order to facilitate diagnosis and stratification as compared to the currently applied *ex vivo* assays, such as immunohistochemistry or fluorescence *in situ* hybridization. Due to their high affinity, many Her2 antibodies serve as pharmaceutical leads for the development of new Her2 tracer molecules, which holds one major disadvantage, though: having very long physical half-lives, antibodies impede the performance of molecular imaging using common radionuclides. [125]. Current approaches rely on the incorporation of long-lived radionuclides, such as ⁸⁹Zr which is characterized by its long physical half-life and its biologic inertness [127]. Nonetheless, ⁸⁹Zr leads to a disadvantageous 2.5-fold higher radiation exposure when compared to conventional FDG-PET [128,129].

In order to decrease the radiation dose, alternative systems have been developed, such as [⁶⁴Cu]-DOTA-trastuzumab. The utilization of ⁶⁴Cu leads to significantly lower radiation doses, as compared to ⁸⁹Zr. Yet, high blood pool activity was observed, making it impossible to detect tumors or metastasis localized next to organs with high blood perfusion, such as heart and liver [130].

Another approach to reduce the radiation exposure is the utilization of alternative binders, such as affibodies [131]. Affibody molecules are small (6.5 kDa) single domain proteins derived from an engineered B-domain of the *Staphylococcus aureus* protein A, which is then called Z-domain [132,133]. It is characterized by high thermal and chemical stability, rapid folding and high solubility [134]. Affibody scaffolds do not contain any cysteine. The introduction of a single cysteine therefore enables site-specific modifications [135].

In 2010, the first Her2-specific Affibody molecule, Z_{Her2:342-pep2} (ABY-002, Affibody AB, Solna, Sweden), was tested in human beings. Two differently radiolabeled variants ([¹¹¹In]-ABY-002 and [⁶⁸Ga]-ABY-002) were applied. Both compounds showed specific tumor uptake and allowed for high contrast imaging of Her2-positive tissue [136]. Nonetheless, a comparative mouse study revealed that [¹¹¹In]-ABY-002 shows high blood pool activity, as well as lung and spleen accumulation [137].

In the last years, the Affibody scaffold of ABY-002 was further modified, in order to increase specificity, stability and to allow site-specific modifications. One of the most promising variants is ABY-025 (maleimide-monomer-DOTA-Cys⁶¹-Z_{Her2:2891}-Cys) [134]. In preclinical animal studies, [¹¹¹In]-ABY-025 could be shown to be neither toxic nor immunogenic [138]. Additionally, it showed high Her2-specificity and affinity ($K_D \approx 76$ pM) [134]. First in-human studies revealed high tolerability of the compound and specific uptake in Her2-positive cancer tissues. High background-uptake was observed for kidneys, liver and spleen [139].

2.8. hNIS

The human sodium iodide symporter (hNIS) is responsible for cellular iodide uptake deploying the physiological sodium gradient. This leads to an intracellular iodide accumulation with concentrations that are 20- to 40-fold higher than in the physiological extracellular environment [140].

hNIS belongs to the group of sodium/solute symporters of the solute carrier 5 family [141,142]. It is mainly expressed in the thyroid, where it imports iodide for the synthesis of the thyroid hormones tri-iodothyronine (T₃) and thyroxine (T₄). Among other effects, these hormones play an important role in the development of the nervous system and the lungs as well as the skeleton and the muscles [142]. High expression levels of hNIS are also seen in the breast tissue of pregnant and lactating women, especially in the lactating mammary gland. The physiological function of hNIS therein is to secrete iodide into the milk, in order to supply the newborn with sufficient amounts of iodide for the synthesis of thyroid hormones [143,144]. In accordance with these findings, hNIS was also found in the placenta, where it ensures the iodide supply of the unborn [145]. Lower, yet detectable, expression levels of hNIS can be found in various tissues, such as the salivary gland [146,147], the testis [148] and the intestines [149].

hNIS is mainly overexpressed in thyroid cancer [150] and estrogen receptor positive breast cancer [151]. Yet, it must be stated that changes in the intracellular trafficking lead to accumulation of hNIS in the cytosol [152]. Thus, neither thyroid cancer nor breast cancer show higher extracellular presence of hNIS when compared to non-cancerous tissue of the same origin. Nonetheless, radioiodine therapy is a powerful tool to reduce hNIS positive diffuse or metastatic thyroid cancer tissue [153]. Additionally, non-cancerous breast tissue is rarely affected by radioiodine therapy or imaging, because hNIS in the breast is only expressed during pregnancy and lactation [154]. In this period of time, radiotherapy is not in compliance with current health care standards [153].

Radioiodine therapy relies on ¹³¹I in order to generate a therapeutic effect. It is applied in the form of sodium iodide [155]. SPECT imaging of hNIS overexpressing tissues is possible by using ¹²³I, instead of the therapeutic radionuclide. ¹²³I imaging is mainly applied for whole body imaging of thyroid cancers [156,157]. Recently, the superiority of ¹²³I over ¹³¹I for SPECT imaging of the thyroid could also be shown [158]. Another approach for the imaging of hNIS overexpressing tissues in thyroid and breast relies on the utilization of ^{99m}Tc-pertechnetate, which also functions as a substrate of hNIS [159,160].

2.9. Prostate Specific Membrane Antigen

The prostate specific membrane antigen (PSMA) is a type II transmembrane glycoprotein and zinc metalloprotease with glutamate-carboxypeptidase functionality, which cleaves the glutamine fraction of folate [161]. PSMA is expressed in low levels on the surface of most prostate cells. Prostate cancer often shows PSMA overexpression [162–164]. PSMA expression is inversely correlated to androgen levels and overexpression is thus seen most often in androgen independent prostate cancer [165,166]. Additionally, PSMA is expressed on the vascular epithelium of different cancer types [167,168].

The exact function of PSMA is yet unknown, but it is thought to play an important role in cell signaling and nutrient uptake [169]. It is also known that PSMA internalizes upon ligand binding via clathrin-dependent endocytosis, which makes it a favorable target for imaging and therapy [170,171].

In the beginning, PSMA was visualized in biopsy and tissue samples by the antibody ^{111}In -capromab pendetide (ProstaScint[®], Cytogen, Princeton, NJ, USA) [172]. *In vivo* imaging using radiolabeled ProstaScint[®] is not possible, because it recognizes an epitope that is localized intracellularly in living cells [173]. Additionally, antibodies are more difficult to handle for *in vivo* imaging purposes, because they show high blood circulation times compared to small molecules. This long physical half-life prolongs the circulation time of the radioisotopes, which thereby damage untargeted tissue [125].

Molecular imaging and targeted therapy finally became possible upon the discovery of structural and, later on, functional correlations of PSMA and the *N*-acetylasparylglutamat peptidase NAALADASE [174,175]. This led to the development of PSMA tracers derived from inhibitors of NAALADASE [176,177]. Currently, most tracer molecules contain the targeting sequence Glu-urea-Lys, where the ϵ -amino group of lysine can be used for site specific modifications.

Recently, a new PSMA tracer was published by Eder *et al.* [178], carrying the acyclic chelator HBED-CC via an aminocaproic acid linker, which ensures reduced interaction between the chelator and the binding pocket of PSMA (see Figure 8). The utilization of HBED-CC has several benefits over other gallium chelators: firstly, it allows quick and stable chelation with ^{68}Ga at low temperatures [179] and secondly, it adds an aromatic moiety to the tracer, which is useful for strong PSMA-tracer interactions and internalization [180]. This property makes PSMA-HBED-CC a valuable tracer for molecular imaging of PSMA-overexpressing cancers.

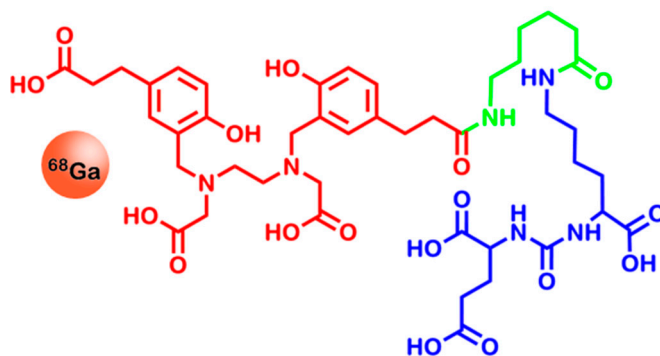


Figure 8. Chemical structure of [^{68}Ga]-PSMA-HBED-CC. The Glu-urea-Lys sequence (blue) is responsible for the targeting properties of the tracer. It is linked to the ^{68}Ga -labeled chelator HBED-CC (red) via an aminocaproic acid linker (green). For reasons of clarity, chelation bonds are omitted.

3. Methods for Molecular Imaging—An Overview

3.1. Computed Tomography (CT)

CT is used to gain information about anatomical structures by monitoring X-ray absorption. The observed differences of intensity depend on the interaction between electromagnetic radiation and solid matter [181]. Additionally, photoelectric absorption correlates with increasing ordinal numbers, which requires the application of contrast agents containing heavy atoms. The most prominent examples are iodine containing CT contrast agents, such as iodixanol (Visipaque[®], GE Healthcare, Buckinghamshire, UK) [182]. In order to generate functional information deploying CT, high amounts of contrast agents have to be applied, which commonly increases side effects [183]. In consequence, CT is currently not considered to become an imaging technique for molecular imaging purposes (see Table 2).

Table 2. Methods used for molecular imaging in oncology [8,184,185].

Method	Spatial Resolution	Temporal Resolution	Sensitivity [mol/L]	Costs	Advantages	Drawbacks
CT	50–200 μm	Minute	–	Low	Generation of anatomical images	It is difficult to generate functional, non-quantitative
MRI	25–100 μm	Minute to hour	10^{-3} – 10^{-5}	Very high	High spatial resolution, non-radioactive tracers	Low sensitivity
PET	2–5 mm	Second to minute	10^{-11} – 10^{-12}	Very high	The most sensitive imaging method, quantitative method, allows to use biologically relevant radionuclides	Imaging of large areas is expensive, low spatial resolution
SPECT	7.5–10 mm	Minute	10^{-10} – 10^{-11}	High	Simultaneous multi-probe imaging is possible	Low spatial resolution

CT: Computed Tomography; MRI: Magnetic Resonance Imaging; PET: Positron Emission Tomography; SPECT: Single Photon Emission Computed Tomography.

3.2. Magnetic Resonance Imaging (MRI)

MRI represents an additional imaging technique for the visualization of anatomical structures, utilizing the proton density and the respective chemical environment of an object [186,187]. Imaging contrast can be increased by using contrast agents carrying paramagnetic or super-paramagnetic substances, which influence the T1 relaxation (transversal relaxation) or the T2 relaxation (longitudinal relaxation) respectively. The most commonly used MRI contrast agents contain gadolinium [188], manganese (both paramagnetic substances) [189], or iron oxide crystals (super-paramagnetic contrast agents) [190]. As in CT, MRI usually requires high amounts of contrast agents in order to gain functional information. This again limits its applicability for molecular imaging purposes [183] (see Table 2).

3.3. Positron Emission Tomography (PET)

PET is the most important method for molecular imaging in oncology [191]. It depends on the detection of gamma rays in order to gain anatomical, as well as functional, information. PET tracers are labeled with radionuclides undergoing β^+ decay and thereby emitting positrons, passing the surrounding tissue for a characteristic distance. Interaction with existent electrons leads to annihilation, resulting in the emission of two collinear γ photons traveling in opposite directions. Thus, the detection of two separate signals at different detectors localized opposite one another is enabled within a very small timeframe. Only such coincident events at opposite positions are monitored and allow the determination of the trajectory on which the annihilation occurred. Monitoring many of these coincident events allows to determine the spatial distribution of the tracer molecule [7].

Additionally, modern PET instruments monitor the time difference between the detected events. This time of flight analysis facilitates a more precise localization of the site of decay [192]. In the last years, multimodality imaging, such as PET/CT became increasingly important, because of their high sensitivity and the possibility to simultaneously generate functional and anatomical data [193,194]. Positron emission is triggered *in vivo* by using tracers containing β^+ emitting radionuclides. Common representatives are ^{11}C , ^{13}N , ^{15}O , ^{18}F , ^{68}Ga and ^{124}I [8,184] (see Table 2).

3.4. Single Photon Emission Computed Tomography (SPECT)

SPECT is a method for molecular imaging that relies on monitoring low energy γ -rays by gamma cameras in order to collect anatomical and functional information. There are three main differences between PET and SPECT: Firstly, PET and SPECT rely on different radionuclides for imaging due to their different imaging processes. In comparison to positron emission tomography, the radiation energy emitted during SPECT is substantially lower (see Table 3). Moreover the emission is measured directly by using single photon emitting radionuclides such as $^{99\text{m}}\text{Tc}$ and ^{111}In ; whereas PET scanners detect coincident events driven by photon pairs [8]. Secondly, PET and SPECT differ in their maximum resolutions, and thirdly in the area they are able to monitor simultaneously [184,195] (see Table 2).

Table 3. Radionuclides used in oncology.

Radionuclide	Decay	Half-Life	Energy	Application	Source
^{11}C	β^+	20 min	511 keV	Diagnosis (PET)	[7]
^{13}N	β^+	10 min	511 keV	Diagnosis (PET)	[7]
^{18}F	β^+	110 min	511 keV	Diagnosis (PET)	[7]
^{64}Cu	β^+	12.7 h	511 keV	Diagnosis (PET)	[7]
^{67}Ga	γ	78 h	93 keV	Diagnosis (SPECT)	[196]
^{68}Ga	β^+	68 min	511 keV	Diagnosis (PET)	[7]
^{86}Y	β^+	14.7 h	511 keV	Diagnosis (PET)	[197]
^{89}Zr	β^+	3.3 days	511 keV	Diagnosis (PET)	[127]
^{90}Y	β^-	2.7 days	2.28 MeV	Therapy	[198]
$^{99\text{m}}\text{Tc}$	γ	6 h	141 keV	Diagnosis (SPECT)	[199]
^{111}In	γ	2.8 days	171 keV	Diagnosis (SPECT)	[199]
^{123}I	γ	13.2 h	159 keV	Diagnosis (SPECT)	[200]
^{124}I	β^+	4.18 days	511 keV	Diagnosis (PET)	[7]

Table 3. *Cont.*

Radionuclide	Decay	Half-Life	Energy	Application	Source
¹³¹ I	β^-	8 days	0.61 MeV	Therapy	[201]
¹⁷⁷ Lu	β^-	6.7 days	0.5 MeV	Therapy	[198]
²⁰¹ Tl	γ	73 h	80 keV	Diagnosis (SPECT)	[202]

4. Conclusions

This article provides an overview of current and future applications of molecular imaging in oncology for the purpose of cancer stratification. Molecular imaging enables non-invasive, simultaneous cancer stratification and localization in the patient. Consequently, its potential differs fundamentally from alternative stratification modalities, such as cancer proteomics and immunohistochemistry. Molecular imaging enables to visually prove the presence of target structures that can be deployed for treatment with highly specific drugs. As radioactive decays can be detected with high sensitivity and accuracy, radiotracers are the most important imaging compounds in modern oncology.

Based on the description of the most commonly used imaging methods in oncology (CT, MRI, PET and SPECT), tumor specific cellular structures and cancer phenotypes are elucidated. For each of these structures, the physiological role, the mode of action, as well as the specific role in cancer development and progression is given to outline their respective prognostic value. Subsequently, specific tracer molecules that target or employ the aforementioned structures are introduced.

A multitude of tracers are already in use for diverse target structures, such as receptors (e.g., somatostatin receptors, folate receptors or Her2), transporters (e.g., glucose transporters, amino acid transporters or hNIS), and cell specific target structures (e.g., PSMA, integrins, and CD20). Moreover, molecular imaging provides information on the functional expression of specific targets which is the basis for the application of theranostics. Examples are Zevalin[®], DOTATOC or the radiotracer-therapeutic pair etarfolatide/vintafolide. In conclusion, molecular imaging plays a steadily increasing role in cancer stratification and contributes significantly to the current development of personalized medicine in cancer therapy.

Author Contributions

Uwe Haberkorn and Walter Mier wrote the vital passages and designed and revised the manuscript. Justus Weber composed the main part of the manuscript and composed the figures.

Conflicts of Interest

The authors declare no conflict of interest.

References

1. Shaw, E.C.; Johnson, P.W.M. Stratified medicine for cancer therapy. *Drug Discov. Today* **2012**, *17*, 261–268.
2. Kulasingam, V.; Diamandis, E.P. Strategies for discovering novel cancer biomarkers through utilization of emerging technologies. *Nat. Clin. Pract. Oncol.* **2008**, *5*, 588–599.

3. Ummanni, R.; Mundt, F.; Pospisil, H.; Venz, S.; Scharf, C.; Barrett, C.; Falth, M.; Kollermann, J.; Walther, R.; Schlomm, T.; *et al.* Identification of clinically relevant protein targets in prostate cancer with 2D-DIGE coupled mass spectrometry and systems biology network platform. *PLoS One* **2011**, *6*, e16833.
4. Palma, P.; Cano, C.; Conde-Muino, R.; Comino, A.; Bueno, P.; Ferron, J.A.; Cuadros, M. Expression profiling of rectal tumors defines response to neoadjuvant treatment related genes. *PLoS One* **2014**, *9*, e112189.
5. Tan, H.T.; Lee, Y.H.; Chung, M.C. Cancer proteomics. *Mass Spectrom. Rev.* **2012**, *31*, 583–605.
6. Uhl, P.; Fricker, G.; Haberkorn, U.; Mier, W. Radionuclides in drug development. *Drug Discov. Today* **2014**, *20*, 198–208.
7. Ametamey, S.M.; Honer, M.; Schubiger, P.A. Molecular imaging with PET. *Chem. Rev.* **2008**, *108*, 1501–1516.
8. Massoud, T.F.; Gambhir, S.S. Molecular imaging in living subjects: Seeing fundamental biological processes in a new light. *Genes Dev.* **2003**, *17*, 545–580.
9. Weissleder, R.; Mahmood, U. Molecular imaging. *Radiology* **2001**, *219*, 316–333.
10. Wright, E.M.; Turk, E. The sodium/glucose cotransport family SLC5. *Pflugers Arch.* **2004**, *447*, 510–518.
11. Macheda, M.L.; Rogers, S.; Best, J.D. Molecular and cellular regulation of glucose transporter (GLUT) proteins in cancer. *J. Cell. Physiol.* **2005**, *202*, 654–662.
12. Joost, H.G.; Bell, G.I.; Best, J.D.; Birnbaum, M.J.; Charron, M.J.; Chen, Y.T.; Doege, H.; James, D.E.; Lodish, H.F.; Moley, K.H.; *et al.* Nomenclature of the GLUT/SLC2A family of sugar/polyol transport facilitators. *Am. J. Physiol. Endocrinol. Metab.* **2002**, *282*, E974–E976.
13. El Sayed, S.M.; Mahmoud, A.A.; El Sawy, S.A.; Abdelaal, E.A.; Fouad, A.M.; Yousif, R.S.; Hashim, M.S.; Hemdan, S.B.; Kadry, Z.M.; Abdelmoaty, M.A.; *et al.* Warburg effect increases steady-state ROS condition in cancer cells through decreasing their antioxidant capacities (anticancer effects of 3-bromopyruvate through antagonizing Warburg effect). *Med. Hypotheses* **2013**, *81*, 866–870.
14. Jang, M.; Kim, S.S.; Lee, J. Cancer cell metabolism: Implications for therapeutic targets. *Exp. Mol. Med.* **2013**, *45*, e45.
15. Mamede, M.; Higashi, T.; Kitaichi, M.; Ishizu, K.; Ishimori, T.; Nakamoto, Y.; Yanagihara, K.; Li, M.; Tanaka, F.; Wada, H.; *et al.* [¹⁸F]FDG uptake and PCNA, Glut-1, and Hexokinase-II expressions in cancers and inflammatory lesions of the lung. *Neoplasia* **2005**, *7*, 369–379.
16. Meller, J.; Sahlmann, C.O.; Scheel, A.K. ¹⁸F-FDG PET and PET/CT in fever of unknown origin. *J. Nucl. Med.* **2007**, *48*, 35–45.
17. Horsman, M.R. Measurement of tumor oxygenation. *Int. J. Radiat. Oncol. Biol. Phys.* **1998**, *42*, 701–704.
18. Ganapathy, V.; Thangaraju, M.; Prasad, P.D. Nutrient transporters in cancer: Relevance to Warburg hypothesis and beyond. *Pharmacol. Ther.* **2009**, *121*, 29–40.
19. Teicher, B.A. Hypoxia and drug resistance. *Cancer Metastasis Rev.* **1994**, *13*, 139–168.
20. Hockel, M.; Schlenger, K.; Aral, B.; Mitze, M.; Schaffer, U.; Vaupel, P. Association between tumor hypoxia and malignant progression in advanced cancer of the uterine cervix. *Cancer Res.* **1996**, *56*, 4509–4515.

21. Berg, J.M.; Tymoczko, J.L.; L., S. Section 17.3, The citric acid cycle is a source of biosynthetic precursors. In *Biochemistry*; W.H. Freeman and Company: New York, NY, USA, 2002.
22. Gatenby, R.A.; Gillies, R.J. Why do cancers have high aerobic glycolysis? *Nat. Rev. Cancer* **2004**, *4*, 891–899.
23. Gatenby, R. Altered glucose metabolism and the invasive tumor phenotype. *Int. J. Oncol.* **1996**, *8*, 597–601.
24. Vegran, F.; Boidot, R.; Michiels, C.; Sonveaux, P.; Feron, O. Lactate influx through the endothelial cell monocarboxylate transporter MCT1 supports an NF- κ B/IL-8 pathway that drives tumor angiogenesis. *Cancer Res.* **2011**, *71*, 2550–2560.
25. Yamamoto, T.; Seino, Y.; Fukumoto, H.; Koh, G.; Yano, H.; Inagaki, N.; Yamada, Y.; Inoue, K.; Manabe, T.; Imura, H. Over-expression of facilitative glucose transporter genes in human cancer. *Biochem. Biophys. Res. Commun.* **1990**, *170*, 223–230.
26. Hennipman, A.; van Oirschot, B.A.; Smits, J.; Rijksen, G.; Staal, G.E. Glycolytic enzyme activities in breast cancer metastases. *Tumour Biol.* **1988**, *9*, 241–248.
27. Brophy, S.; Sheehan, K.M.; McNamara, D.A.; Deasy, J.; Bouchier-Hayes, D.J.; Kay, E.W. GLUT-1 expression and response to chemoradiotherapy in rectal cancer. *Int. J. Cancer* **2009**, *125*, 2778–2782.
28. Smith, T.A. FDG uptake, tumour characteristics and response to therapy: A review. *Nucl. Med. Commun.* **1998**, *19*, 97–105.
29. Pauwels, E.K.; Ribeiro, M.J.; Stoot, J.H.; McCready, V.R.; Bourguignon, M.; Maziere, B. FDG accumulation and tumor biology. *Nucl. Med. Biol.* **1998**, *25*, 317–322.
30. Nelson, C.A.; Wang, J.Q.; Leav, I.; Crane, P.D. The interaction among glucose transport, hexokinase, and glucose-6-phosphatase with respect to 3H-2-deoxyglucose retention in murine tumor models. *Nucl. Med. Biol.* **1996**, *23*, 533–541.
31. Baumann, M.; Jezussek, D.; Lang, T.; Richter, R.T.; Brand, K. Activities of phosphohexose isomerase and other glycolytic enzymes in normal and tumor tissue of patients with neoplastic diseases: Comparison with serum activities and correlation to tumor staging and grading. *Tumour Biol.* **1988**, *9*, 281–286.
32. Im, H.J.; Pak, K.; Cheon, G.J.; Kang, K.W.; Kim, S.J.; Kim, I.J.; Chung, J.K.; Kim, E.E.; Lee, D.S. Prognostic value of volumetric parameters of 18 F-FDG PET in non-small-cell lung cancer: A meta-analysis. *Eur. J. Nucl. Med. Mol. Imaging* **2014**, *42*, 241–251.
33. Iakovou, I.P.; Giannoula, E. [Nuclear medicine in diagnosis of breast cancer]. *Hell. J. Nucl. Med.* **2014**, *17*, 221–227.
34. Win, A.Z. Renal cell carcinoma metastasis to the gallbladder detected by FDG-PET/CT. *J. Clin. Med. Res.* **2014**, *6*, 482–486.
35. Gallamini, A.; Zwarthoed, C.; Borra, A. Positron emission tomography (PET) in oncology. *Cancers (Basel)* **2014**, *6*, 1821–1889.
36. Hawkins, R.A.; Hoh, C.K. PET FDG studies in oncology. *Nucl. Med. Biol.* **1994**, *21*, 739–747.
37. Fotiadis, D.; Kanai, Y.; Palacin, M. The SLC3 and SLC7 families of amino acid transporters. *Mol. Asp. Med.* **2013**, *34*, 139–158.
38. Closs, E.I.; Boissel, J.P.; Habermeier, A.; Rotmann, A. Structure and function of cationic amino acid transporters (CATs). *J. Membr. Biol.* **2006**, *213*, 67–77.

39. Closs, E.I. Expression, regulation and function of carrier proteins for cationic amino acids. *Curr. Opin. Nephrol. Hypertens.* **2002**, *11*, 99–107.
40. Closs, E.I.; Lyons, C.R.; Kelly, C.; Cunningham, J.M. Characterization of the third member of the MCAT family of cationic amino acid transporters. Identification of a domain that determines the transport properties of the MCAT proteins. *J. Biol. Chem.* **1993**, *268*, 20796–20800.
41. Yanagida, O.; Kanai, Y.; Chairoungdua, A.; Kim, D.K.; Segawa, H.; Nii, T.; Cha, S.H.; Matsuo, H.; Fukushima, J.; Fukasawa, Y.; *et al.* Human L-type amino acid transporter 1 (LAT1): Characterization of function and expression in tumor cell lines. *Biochim. Biophys. Acta* **2001**, *1514*, 291–302.
42. Kanai, Y.; Segawa, H.; Miyamoto, K.; Uchino, H.; Takeda, E.; Endou, H. Expression cloning and characterization of a transporter for large neutral amino acids activated by the heavy chain of 4F2 antigen (CD98). *J. Biol. Chem.* **1998**, *273*, 23629–23632.
43. Fort, J.; de la Ballina, L.R.; Burghardt, H.E.; Ferrer-Costa, C.; Turnay, J.; Ferrer-Orta, C.; Uson, I.; Zorzano, A.; Fernandez-Recio, J.; Orozco, M.; *et al.* The structure of human 4F2hc ectodomain provides a model for homodimerization and electrostatic interaction with plasma membrane. *J. Biol. Chem.* **2007**, *282*, 31444–31452.
44. Palacin, M.; Kanai, Y. The ancillary proteins of HATs: SLC3 family of amino acid transporters. *Pflugers Arch.* **2004**, *447*, 490–494.
45. Uno, K.; Kuwabara, H.; Terado, Y.; Kojima, K.; Kawakami, T.; Kamma, H.; Sakurai, H.; Sakamoto, A.; Kurata, A. Divergent expression of L-type amino acid transporter 1 during uterine cervical carcinogenesis. *Hum. Pathol.* **2011**, *42*, 1660–1666.
46. Ichinoe, M.; Mikami, T.; Yoshida, T.; Igawa, I.; Tsuruta, T.; Nakada, N.; Anzai, N.; Suzuki, Y.; Endou, H.; Okayasu, I. High expression of L-type amino-acid transporter 1 (LAT1) in gastric carcinomas: Comparison with non-cancerous lesions. *Pathol. Int.* **2011**, *61*, 281–289.
47. Yoon, J.H.; Kim, I.J.; Kim, H.; Kim, H.J.; Jeong, M.J.; Ahn, S.G.; Kim, S.A.; Lee, C.H.; Choi, B.K.; Kim, J.K.; *et al.* Amino acid transport system L is differently expressed in human normal oral keratinocytes and human oral cancer cells. *Cancer Lett.* **2005**, *222*, 237–245.
48. Kaira, K.; Oriuchi, N.; Imai, H.; Shimizu, K.; Yanagitani, N.; Sunaga, N.; Hisada, T.; Tanaka, S.; Ishizuka, T.; Kanai, Y.; *et al.* Prognostic significance of L-type amino acid transporter 1 expression in resectable stage I–III nonsmall cell lung cancer. *Br. J. Cancer* **2008**, *98*, 742–748.
49. Kaira, K.; Oriuchi, N.; Takahashi, T.; Nakagawa, K.; Ohde, Y.; Okumura, T.; Murakami, H.; Shukuya, T.; Kenmotsu, H.; Naito, T.; *et al.* L-type amino acid transporter 1 (LAT1) expression in malignant pleural mesothelioma. *Anticancer Res.* **2011**, *31*, 4075–4082.
50. Kekuda, R.; Prasad, P.D.; Fei, Y.J.; Torres-Zamorano, V.; Sinha, S.; Yang-Feng, T.L.; Leibach, F.H.; Ganapathy, V. Cloning of the sodium-dependent, broad-scope, neutral amino acid transporter Bo from a human placental choriocarcinoma cell line. *J. Biol. Chem.* **1996**, *271*, 18657–18661.
51. Fuchs, B.C.; Bode, B.P. Amino acid transporters ASCT2 and LAT1 in cancer: Partners in crime? *Semin. Cancer Biol.* **2005**, *15*, 254–266.
52. Li, R.; Younes, M.; Frolov, A.; Wheeler, T.M.; Scardino, P.; Otori, M.; Ayala, G. Expression of neutral amino acid transporter ASCT2 in human prostate. *Anticancer Res.* **2003**, *23*, 3413–3418.
53. Sundin, A.; Garske, U.; Orlefors, H. Nuclear imaging of neuroendocrine tumours. *Best Pract. Res. Clin. Endocrinol. Metab.* **2007**, *21*, 69–85.

54. Huang, C.; McConathy, J. Radiolabeled amino acids for oncologic imaging. *J. Nucl. Med.* **2013**, *54*, 1007–1010.
55. McConathy, J.; Yu, W.; Jarkas, N.; Seo, W.; Schuster, D.M.; Goodman, M.M. Radiohalogenated nonnatural amino acids as PET and SPECT tumor imaging agents. *Med. Res. Rev.* **2012**, *32*, 868–905.
56. Shikano, N.; Kanai, Y.; Kawai, K.; Inatomi, J.; Kim, D.K.; Ishikawa, N.; Endou, H. Isoform selectivity of 3–125I-iodo- α -methyl-L-tyrosine membrane transport in human L-type amino acid transporters. *J. Nucl. Med.* **2003**, *44*, 244–246.
57. Pauleit, D.; Floeth, F.; Tellmann, L.; Hamacher, K.; Hautzel, H.; Muller, H.W.; Coenen, H.H.; Langen, K.J. Comparison of O-(2–18F-fluoroethyl)-L-tyrosine PET and 3–123I-iodo- α -methyl-L-tyrosine SPECT in brain tumors. *J. Nucl. Med.* **2004**, *45*, 374–381.
58. Wiriyasermkul, P.; Nagamori, S.; Tominaga, H.; Oriuchi, N.; Kaira, K.; Nakao, H.; Kitashoji, T.; Ohgaki, R.; Tanaka, H.; Endou, H.; *et al.* Transport of 3-fluoro-L- α -methyl-tyrosine by tumor-upregulated L-type amino acid transporter 1: A cause of the tumor uptake in PET. *J. Nucl. Med.* **2012**, *53*, 1253–1261.
59. Kaira, K.; Oriuchi, N.; Shimizu, K.; Ishikita, T.; Higuchi, T.; Imai, H.; Yanagitani, N.; Sunaga, N.; Hisada, T.; Ishizuka, T.; *et al.* Correlation of angiogenesis with 18F-FMT and 18F-FDG uptake in non-small cell lung cancer. *Cancer Sci.* **2009**, *100*, 753–758.
60. Imai, H.; Kaira, K.; Oriuchi, N.; Shimizu, K.; Tominaga, H.; Yanagitani, N.; Sunaga, N.; Ishizuka, T.; Nagamori, S.; Promchan, K.; *et al.* Inhibition of L-type amino acid transporter 1 has antitumor activity in non-small cell lung cancer. *Anticancer Res.* **2010**, *30*, 4819–4828.
61. Brazeau, P.; Vale, W.; Burgus, R.; Ling, N.; Butcher, M.; Rivier, J.; Guillemin, R. Hypothalamic polypeptide that inhibits the secretion of immunoreactive pituitary growth hormone. *Science* **1973**, *179*, 77–79.
62. Reichlin, S. Secretion of somatostatin and its physiologic function. *J. Lab. Clin. Med.* **1987**, *109*, 320–326.
63. Reubi, J.C.; Waser, B.; Liu, Q.; Laissue, J.A.; Schonbrunn, A. Subcellular distribution of somatostatin sst2A receptors in human tumors of the nervous and neuroendocrine systems: Membranous *versus* intracellular location. *J. Clin. Endocrinol. Metab.* **2000**, *85*, 3882–3891.
64. Lüllmann, H.; Mohr, K.; Hein, L. Hormonsystem. In *Pharmakologie und Toxikologie*, 2010; Volume 17, pp. 395–451.
65. Reubi, J.C.; Waser, B.; Schaer, J.C.; Laissue, J.A. Somatostatin receptor sst1–sst5 expression in normal and neoplastic human tissues using receptor autoradiography with subtype-selective ligands. *Eur. J. Nucl. Med.* **2001**, *28*, 836–846.
66. Nouel, D.; Gaudriault, G.; Houle, M.; Reisine, T.; Vincent, J.P.; Mazella, J.; Beaudet, A. Differential internalization of somatostatin in COS-7 cells transfected with SST1 and SST2 receptor subtypes: A confocal microscopic study using novel fluorescent somatostatin derivatives. *Endocrinology* **1997**, *138*, 296–306.
67. Reichlin, S. Somatostatin. *N. Engl. J. Med.* **1983**, *309*, 1495–1501.
68. Delaunoit, T.; Rubin, J.; Neczyporenko, F.; Erlichman, C.; Hobday, T.J. Somatostatin analogues in the treatment of gastroenteropancreatic neuroendocrine tumors. *Mayo Clin. Proc.* **2005**, *80*, 502–506.

69. Vale, W.; Rivier, J.; Ling, N.; Brown, M. Biologic and immunologic activities and applications of somatostatin analogs. *Metabolism* **1978**, *27*, 1391–1401.
70. Bauer, W.; Briner, U.; Doepfner, W.; Haller, R.; Huguenin, R.; Marbach, P.; Petcher, T.J.; Pless, J. SMS 201–995: A very potent and selective octapeptide analogue of somatostatin with prolonged action. *Life Sci.* **1982**, *31*, 1133–1140.
71. Modlin, I.M.; Pavel, M.; Kidd, M.; Gustafsson, B.I. Review article: Somatostatin analogues in the treatment of gastroenteropancreatic neuroendocrine (carcinoid) tumours. *Aliment. Pharmacol. Ther.* **2010**, *31*, 169–188.
72. Frilling, A.; Weber, F.; Saner, F.; Bockisch, A.; Hofmann, M.; Mueller-Brand, J.; Broelsch, C.E. Treatment with (90)Y- and (177)Lu-DOTATOC in patients with metastatic neuroendocrine tumors. *Surgery* **2006**, *140*, 968–976.
73. Antunes, P.; Ginj, M.; Zhang, H.; Waser, B.; Baum, R.P.; Reubi, J.C.; Maecke, H. Are radiogallium-labelled DOTA-conjugated somatostatin analogues superior to those labelled with other radiometals? *Eur. J. Nucl. Med. Mol. Imaging* **2007**, *34*, 982–993.
74. Froidevaux, S.; Eberle, A.N.; Christe, M.; Sumanovski, L.; Heppeler, A.; Schmitt, J.S.; Eisenwiener, K.; Beglinger, C.; Macke, H.R. Neuroendocrine tumor targeting: Study of novel gallium-labeled somatostatin radiopeptides in a rat pancreatic tumor model. *Int. J. Cancer* **2002**, *98*, 930–937.
75. Bruns, C.; Lewis, I.; Briner, U.; Meno-Tetang, G.; Weckbecker, G. SOM230: A novel somatostatin peptidomimetic with broad somatotropin release inhibiting factor (SRIF) receptor binding and a unique antisecretory profile. *Eur. J. Endocrinol.* **2002**, *146*, 707–716.
76. Takada, Y.; Ye, X.; Simon, S. The integrins. *Genome Biol.* **2007**, *8*, 215.
77. Hynes, R.O. Integrins: Bidirectional, allosteric signaling machines. *Cell* **2002**, *110*, 673–687.
78. Luo, B.H.; Carman, C.V.; Springer, T.A. Structural basis of integrin regulation and signaling. *Annu. Rev. Immunol.* **2007**, *25*, 619–647.
79. Barczyk, M.; Carracedo, S.; Gullberg, D. Integrins. *Cell. Tissue Res.* **2010**, *339*, 269–280.
80. Guo, W.; Giancotti, F.G. Integrin signalling during tumour progression. *Nat. Rev. Mol. Cell. Biol.* **2004**, *5*, 816–826.
81. Miranti, C.K.; Brugge, J.S. Sensing the environment: A historical perspective on integrin signal transduction. *Nat. Cell. Biol.* **2002**, *4*, E83–E90.
82. Hsu, M.Y.; Shih, D.T.; Meier, F.E.; van Belle, P.; Hsu, J.Y.; Elder, D.E.; Buck, C.A.; Herlyn, M. Adenoviral gene transfer of $\beta 3$ integrin subunit induces conversion from radial to vertical growth phase in primary human melanoma. *Am. J. Pathol.* **1998**, *153*, 1435–1442.
83. Cai, W.; Niu, G.; Chen, X. Imaging of integrins as biomarkers for tumor angiogenesis. *Curr. Pharm. Des.* **2008**, *14*, 2943–2973.
84. Gladson, C.L.; Cheresch, D.A. Glioblastoma expression of vitronectin and the $\alpha \beta 3$ integrin. Adhesion mechanism for transformed glial cells. *J. Clin. Investig.* **1991**, *88*, 1924–1932.
85. Albelda, S.M.; Mette, S.A.; Elder, D.E.; Stewart, R.; Damjanovich, L.; Herlyn, M.; Buck, C.A. Integrin distribution in malignant melanoma: Association of the $\beta 3$ subunit with tumor progression. *Cancer Res.* **1990**, *50*, 6757–6764.

86. Sutcliffe-Goulden, J.L.; O'Doherty, M.J.; Marsden, P.K.; Hart, I.R.; Marshall, J.F.; Bansal, S.S. Rapid solid phase synthesis and biodistribution of ^{18}F -labelled linear peptides. *Eur. J. Nucl. Med. Mol. Imaging* **2002**, *29*, 754–759.
87. Cai, H.; Conti, P.S. RGD-based PET tracers for imaging receptor integrin $\alpha\text{v}\beta\text{3}$ expression. *J. Label. Compd. Radiopharm.* **2013**, *56*, 264–279.
88. Aumailley, M.; Gurrath, M.; Muller, G.; Calvete, J.; Timpl, R.; Kessler, H. Arg-Gly-Asp constrained within cyclic pentapeptides. Strong and selective inhibitors of cell adhesion to vitronectin and laminin fragment P1. *FEBS Lett.* **1991**, *291*, 50–54.
89. Haubner, R.H.; Wester, H.J.; Weber, W.A.; Schwaiger, M. Radiotracer-based strategies to image angiogenesis. *Q. J. Nucl. Med.* **2003**, *47*, 189–199.
90. Wadas, T.J.; Wong, E.H.; Weisman, G.R.; Anderson, C.J. Coordinating radiometals of copper, gallium, indium, yttrium, and zirconium for PET and SPECT imaging of disease. *Chem. Rev.* **2010**, *110*, 2858–2902.
91. Decristoforo, C.; Hernandez Gonzalez, I.; Carlsen, J.; Rupprich, M.; Huisman, M.; Virgolini, I.; Wester, H.J.; Haubner, R. ^{68}Ga - and ^{111}In -labelled DOTA-RGD peptides for imaging of $\alpha\text{v}\beta\text{3}$ integrin expression. *Eur. J. Nucl. Med. Mol. Imaging* **2008**, *35*, 1507–1515.
92. Knetsch, P.A.; Petrik, M.; Griessinger, C.M.; Rangger, C.; Fani, M.; Kesenheimer, C.; von Guggenberg, E.; Pichler, B.J.; Virgolini, I.; Decristoforo, C.; *et al.* [^{68}Ga]NODAGA-RGD for imaging $\alpha\text{v}\beta\text{3}$ integrin expression. *Eur. J. Nucl. Med. Mol. Imaging* **2011**, *38*, 1303–1312.
93. Davis, R.E.; Nicol, D.J. Folic acid. *Int. J. Biochem.* **1988**, *20*, 133–139.
94. Zhao, R.; Matherly, L.H.; Goldman, I.D. Membrane transporters and folate homeostasis: Intestinal absorption and transport into systemic compartments and tissues. *Expert Rev. Mol. Med.* **2009**, *11*, e4.
95. Westerhof, G.R.; Rijnboutt, S.; Schornagel, J.H.; Pinedo, H.M.; Peters, G.J.; Jansen, G. Functional activity of the reduced folate carrier in KB, MA104, and IGROV-I cells expressing folate-binding protein. *Cancer Res.* **1995**, *55*, 3795–3802.
96. Qiu, A.; Jansen, M.; Sakaris, A.; Min, S.H.; Chattopadhyay, S.; Tsai, E.; Sandoval, C.; Zhao, R.; Akabas, M.H.; Goldman, I.D. Identification of an intestinal folate transporter and the molecular basis for hereditary folate malabsorption. *Cell* **2006**, *127*, 917–928.
97. Wang, X.; Shen, F.; Freisheim, J.H.; Gentry, L.E.; Ratnam, M. Differential stereospecificities and affinities of folate receptor isoforms for folate compounds and antifolates. *Biochem. Pharmacol.* **1992**, *44*, 1898–1901.
98. Rothberg, K.G.; Ying, Y.S.; Kolhouse, J.F.; Kamen, B.A.; Anderson, R.G. The glycopospholipid-linked folate receptor internalizes folate without entering the clathrin-coated pit endocytic pathway. *J. Cell Biol.* **1990**, *110*, 637–649.
99. Toffoli, G.; Cernigoi, C.; Russo, A.; Gallo, A.; Bagnoli, M.; Boiocchi, M. Overexpression of folate binding protein in ovarian cancers. *Int. J. Cancer* **1997**, *74*, 193–198.
100. Garin-Chesa, P.; Campbell, I.; Saigo, P.E.; Lewis, J.L., Jr.; Old, L.J.; Rettig, W.J. Trophoblast and ovarian cancer antigen LK26. Sensitivity and specificity in immunopathology and molecular identification as a folate-binding protein. *Am. J. Pathol.* **1993**, *142*, 557–567.
101. Sudimack, J.; Lee, R.J. Targeted drug delivery via the folate receptor. *Adv. Drug Deliv. Rev.* **2000**, *41*, 147–162.

102. Gigant, B.; Wang, C.; Ravelli, R.B.; Roussi, F.; Steinmetz, M.O.; Curmi, P.A.; Sobel, A.; Knossow, M. Structural basis for the regulation of tubulin by vinblastine. *Nature* **2005**, *435*, 519–522.
103. Marchetti, C.; Palaia, I.; Giorgini, M.; de Medici, C.; Iadarola, R.; Vertechy, L.; Domenici, L.; di Donato, V.; Tomao, F.; Muzii, L.; *et al.* Targeted drug delivery via folate receptors in recurrent ovarian cancer: A review. *OncoTargets Ther.* **2014**, *7*, 1223–1236.
104. Maurer, A.H.; Elsinga, P.; Fanti, S.; Nguyen, B.; Oyen, W.J.; Weber, W.A. Imaging the folate receptor on cancer cells with ^{99m}Tc-etarfolatide: Properties, clinical use, and future potential of folate receptor imaging. *J. Nucl. Med.* **2014**, *55*, 701–704.
105. Morris, R.T.; Joyrich, R.N.; Naumann, R.W.; Shah, N.P.; Maurer, A.H.; Strauss, H.W.; Uszler, J.M.; Symanowski, J.T.; Ellis, P.R.; Harb, W.A. Phase II study of treatment of advanced ovarian cancer with folate-receptor-targeted therapeutic (vintafolide) and companion SPECT-based imaging agent (^{99m}Tc-etarfolatide). *Ann. Oncol.* **2014**, *25*, 852–858.
106. Naumann, R.W.; Coleman, R.L.; Burger, R.A.; Sausville, E.A.; Kutarska, E.; Ghamande, S.A.; Gabrail, N.Y.; Depasquale, S.E.; Nowara, E.; Gilbert, L.; *et al.* PRECEDENT: A randomized phase II trial comparing vintafolide (EC145) and pegylated liposomal doxorubicin (PLD) in combination *versus* PLD alone in patients with platinum-resistant ovarian cancer. *J. Clin. Oncol.* **2013**, *31*, 4400–4406.
107. Reff, M.E.; Carner, K.; Chambers, K.S.; Chinn, P.C.; Leonard, J.E.; Raab, R.; Newman, R.A.; Hanna, N.; Anderson, D.R. Depletion of B cells *in vivo* by a chimeric mouse human monoclonal antibody to CD20. *Blood* **1994**, *83*, 435–445.
108. Anderson, K.C.; Bates, M.P.; Slaughenhaupt, B.L.; Pinkus, G.S.; Schlossman, S.F.; Nadler, L.M. Expression of human B cell-associated antigens on leukemias and lymphomas: A model of human B cell differentiation. *Blood* **1984**, *63*, 1424–1433.
109. Tedder, T.F.; Boyd, A.W.; Freedman, A.S.; Nadler, L.M.; Schlossman, S.F. The B cell surface molecule B1 is functionally linked with B cell activation and differentiation. *J. Immunol.* **1985**, *135*, 973–979.
110. Golay, J.T.; Clark, E.A.; Beverley, P.C. The CD20 (Bp35) antigen is involved in activation of B cells from the G₀ to the G₁ phase of the cell cycle. *J. Immunol.* **1985**, *135*, 3795–3801.
111. Kanzaki, M.; Shibata, H.; Mogami, H.; Kojima, I. Expression of calcium-permeable cation channel CD20 accelerates progression through the G₁ phase in Balb/c 3T3 cells. *J. Biol. Chem.* **1995**, *270*, 13099–13104.
112. Kanzaki, M.; Lindorfer, M.A.; Garrison, J.C.; Kojima, I. Activation of the calcium-permeable cation channel CD20 by α subunits of the G_i protein. *J. Biol. Chem.* **1997**, *272*, 14733–14739.
113. Golay, J.; Cusmano, G.; Introna, M. Independent regulation of *c-myc*, *B-myb*, and *c-myb* gene expression by inducers and inhibitors of proliferation in human B lymphocytes. *J. Immunol.* **1992**, *149*, 300–308.
114. White, M.W.; McConnell, F.; Shu, G.L.; Morris, D.R.; Clark, E.A. Activation of dense human tonsillar B cells. Induction of *c-myc* gene expression via two distinct signal transduction pathways. *J. Immunol.* **1991**, *146*, 846–853.
115. Von Schilling, C. Immunotherapy with anti-CD20 compounds. *Semin. Cancer Biol.* **2003**, *13*, 211–222.

116. Maloney, D.G. Anti-CD20 antibody therapy for B-cell lymphomas. *N. Engl. J. Med.* **2012**, *366*, 2008–2016.
117. Gatter, K.; Warnke, R. Diffuse large B cell lymphoma. In *Pathology and Genetics of Tumors of Haematopoietic and Lymphoid Tissues*; Jaffe, E., Harris, N., Stein, H., Vardiman, J., Eds.; IARC Press: Lyon, France, 2001.
118. Goldsmith, S.J. Radioimmunotherapy of lymphoma: Bexxar and Zevalin. *Semin. Nucl. Med.* **2010**, *40*, 122–135.
119. Witzig, T.E.; Gordon, L.I.; Cabanillas, F.; Czuczman, M.S.; Emmanouilides, C.; Joyce, R.; Pohlman, B.L.; Bartlett, N.L.; Wiseman, G.A.; Padre, N.; *et al.* Randomized controlled trial of yttrium-90-labeled ibritumomab tiuxetan radioimmunotherapy *versus* rituximab immunotherapy for patients with relapsed or refractory low-grade, follicular, or transformed B-cell non-Hodgkin's lymphoma. *J. Clin. Oncol.* **2002**, *20*, 2453–2463.
120. Conti, P.S.; White, C.; Pieslor, P.; Molina, A.; Aussie, J.; Foster, P. The role of imaging with ¹¹¹In-ibritumomab tiuxetan in the ibritumomab tiuxetan (Zevalin) regimen: Results from a Zevalin imaging registry. *J. Nucl. Med.* **2005**, *46*, 1812–1818.
121. Citri, A.; Yarden, Y. EGF-ERBB signalling: Towards the systems level. *Nat. Rev. Mol. Cell. Biol.* **2006**, *7*, 505–516.
122. Hynes, N.E.; Lane, H.A. ERBB receptors and cancer: The complexity of targeted inhibitors. *Nat. Rev. Cancer* **2005**, *5*, 341–354.
123. Scholl, S.; Beuzeboc, P.; Pouillart, P. Targeting HER2 in other tumor types. *Ann. Oncol.* **2001**, *12*, S81–S87.
124. Ignatiadis, M.; Desmedt, C.; Sotiriou, C.; de Azambuja, E.; Piccart, M. HER-2 as a target for breast cancer therapy. *Clin. Cancer Res.* **2009**, *15*, 1848–1852.
125. Capala, J.; Bouchelouche, K. Molecular imaging of HER2-positive breast cancer: A step toward an individualized “image and treat” strategy. *Curr. Opin. Oncol.* **2010**, *22*, 559–566.
126. Chari, R.V.; Miller, M.L.; Widdison, W.C. Antibody-drug conjugates: An emerging concept in cancer therapy. *Angew. Chem. Int. Ed. Engl.* **2014**, *53*, 3796–3827.
127. Zhang, Y.; Hong, H.; Cai, W. PET tracers based on Zirconium-89. *Curr. Radiopharm.* **2011**, *4*, 131–139.
128. Dijkers, E.C.; Kosterink, J.G.; Rademaker, A.P.; Perk, L.R.; van Dongen, G.A.; Bart, J.; de Jong, J.R.; de Vries, E.G.; Lub-de Hooge, M.N. Development and characterization of clinical-grade ⁸⁹Zr-trastuzumab for HER2/*neu* immunoPET imaging. *J. Nucl. Med.* **2009**, *50*, 974–981.
129. Dijkers, E.C.; Oude Munnink, T.H.; Kosterink, J.G.; Brouwers, A.H.; Jager, P.L.; de Jong, J.R.; van Dongen, G.A.; Schroder, C.P.; Lub-de Hooge, M.N.; de Vries, E.G. Biodistribution of ⁸⁹Zr-trastuzumab and PET imaging of HER2-positive lesions in patients with metastatic breast cancer. *Clin. Pharmacol. Ther.* **2010**, *87*, 586–592.
130. Tamura, K.; Kurihara, H.; Yonemori, K.; Tsuda, H.; Suzuki, J.; Kono, Y.; Honda, N.; Kodaira, M.; Yamamoto, H.; Yunokawa, M.; *et al.* ⁶⁴Cu-DOTA-trastuzumab PET imaging in patients with HER2-positive breast cancer. *J. Nucl. Med.* **2013**, *54*, 1869–1875.
131. Lofblom, J.; Feldwisch, J.; Tolmachev, V.; Carlsson, J.; Stahl, S.; Frejd, F.Y. Affibody molecules: Engineered proteins for therapeutic, diagnostic and biotechnological applications. *FEBS Lett.* **2010**, *584*, 2670–2680.

132. Uhlen, M.; Guss, B.; Nilsson, B.; Gatenbeck, S.; Philipson, L.; Lindberg, M. Complete sequence of the staphylococcal gene encoding protein A. A gene evolved through multiple duplications. *J. Biol. Chem.* **1984**, *259*, 1695–1702.
133. Nilsson, B.; Moks, T.; Jansson, B.; Abrahmsen, L.; Elmlblad, A.; Holmgren, E.; Henrichson, C.; Jones, T.A.; Uhlen, M. A synthetic IgG-binding domain based on staphylococcal protein A. *Protein Eng.* **1987**, *1*, 107–113.
134. Feldwisch, J.; Tolmachev, V.; Lendel, C.; Herne, N.; Sjoberg, A.; Larsson, B.; Rosik, D.; Lindqvist, E.; Fant, G.; Hoiden-Guthenberg, I.; *et al.* Design of an optimized scaffold for affibody molecules. *J. Mol. Biol.* **2010**, *398*, 232–247.
135. Lundberg, E.; Hoiden-Guthenberg, I.; Larsson, B.; Uhlen, M.; Graslund, T. Site-specifically conjugated anti-HER2 Affibody molecules as one-step reagents for target expression analyses on cells and xenograft samples. *J. Immunol. Methods* **2007**, *319*, 53–63.
136. Baum, R.P.; Prasad, V.; Muller, D.; Schuchardt, C.; Orlova, A.; Wennborg, A.; Tolmachev, V.; Feldwisch, J. Molecular imaging of HER2-expressing malignant tumors in breast cancer patients using synthetic ¹¹¹In- or ⁶⁸Ga-labeled affibody molecules. *J. Nucl. Med.* **2010**, *51*, 892–897.
137. Tolmachev, V.; Velikyan, I.; Sandstrom, M.; Orlova, A. A HER2-binding Affibody molecule labelled with ⁶⁸Ga for PET imaging: Direct *in vivo* comparison with the ¹¹¹In-labelled analogue. *Eur. J. Nucl. Med. Mol. Imaging* **2010**, *37*, 1356–1367.
138. Ahlgren, S.; Orlova, A.; Wallberg, H.; Hansson, M.; Sandstrom, M.; Lewsley, R.; Wennborg, A.; Abrahmsen, L.; Tolmachev, V.; Feldwisch, J. Targeting of HER2-expressing tumors using ¹¹¹In-ABY-025, a second-generation affibody molecule with a fundamentally reengineered scaffold. *J. Nucl. Med.* **2010**, *51*, 1131–1138.
139. Sorensen, J.; Sandberg, D.; Sandstrom, M.; Wennborg, A.; Feldwisch, J.; Tolmachev, V.; Astrom, G.; Lubberink, M.; Garske-Roman, U.; Carlsson, J.; *et al.* First-in-human molecular imaging of HER2 expression in breast cancer metastases using the ¹¹¹In-ABY-025 affibody molecule. *J. Nucl. Med.* **2014**, *55*, 730–735.
140. Rodriguez, A.M.; Perron, B.; Lacroix, L.; Caillou, B.; Leblanc, G.; Schlumberger, M.; Bidart, J.M.; Pourcher, T. Identification and characterization of a putative human iodide transporter located at the apical membrane of thyrocytes. *J. Clin. Endocrinol. Metab.* **2002**, *87*, 3500–3503.
141. Jung, H. The sodium/substrate symporter family: Structural and functional features. *FEBS Lett.* **2002**, *529*, 73–77.
142. De La Vieja, A.; Dohan, O.; Levy, O.; Carrasco, N. Molecular analysis of the sodium/iodide symporter: Impact on thyroid and extrathyroid pathophysiology. *Physiol. Rev.* **2000**, *80*, 1083–1105.
143. Dohan, O.; Carrasco, N. Advances in Na⁺/I⁻ symporter (NIS) research in the thyroid and beyond. *Mol. Cell. Endocrinol.* **2003**, *213*, 59–70.
144. Dadachova, E.; Carrasco, N. The Na/I symporter (NIS): Imaging and therapeutic applications. *Semin. Nucl. Med.* **2004**, *34*, 23–31.
145. Mitchell, A.M.; Manley, S.W.; Morris, J.C.; Powell, K.A.; Bergert, E.R.; Mortimer, R.H. Sodium iodide symporter (NIS) gene expression in human placenta. *Placenta* **2001**, *22*, 256–258.
146. Jhiang, S.M.; Cho, J.Y.; Ryu, K.Y.; de Young, B.R.; Smanik, P.A.; McGaughy, V.R.; Fischer, A.H.; Mazzaferri, E.L. An immunohistochemical study of Na⁺/I⁻ symporter in human thyroid tissues and salivary gland tissues. *Endocrinology* **1998**, *139*, 4416–4419.

147. La Perle, K.M.; Kim, D.C.; Hall, N.C.; Bobbey, A.; Shen, D.H.; Nagy, R.S.; Wakely, P.E., Jr.; Lehman, A.; Jarjoura, D.; Jhiang, S.M. Modulation of sodium/iodide symporter expression in the salivary gland. *Thyroid* **2013**, *23*, 1029–1036.
148. Russo, D.; Scipioni, A.; Durante, C.; Ferretti, E.; Gandini, L.; Maggisano, V.; Paoli, D.; Verrienti, A.; Costante, G.; Lenzi, A.; *et al.* Expression and localization of the sodium/iodide symporter (NIS) in testicular cells. *Endocrine* **2011**, *40*, 35–40.
149. Nicola, J.P.; Basquin, C.; Portulano, C.; Reyna-Neyra, A.; Paroder, M.; Carrasco, N. The Na⁺/I⁻ symporter mediates active iodide uptake in the intestine. *Am. J. Physiol. Cell. Physiol.* **2009**, *296*, C654–C662.
150. Saito, T.; Endo, T.; Kawaguchi, A.; Ikeda, M.; Katoh, R.; Kawaoi, A.; Muramatsu, A.; Onaya, T. Increased expression of the sodium/iodide symporter in papillary thyroid carcinomas. *J. Clin. Investig.* **1998**, *101*, 1296–1300.
151. Chatterjee, S.; Malhotra, R.; Varghese, F.; Bukhari, A.B.; Patil, A.; Budrukkar, A.; Parmar, V.; Gupta, S.; De, A. Quantitative immunohistochemical analysis reveals association between sodium iodide symporter and estrogen receptor expression in breast cancer. *PLoS One* **2013**, *8*, e54055.
152. Dohan, O.; Baloch, Z.; Banrevi, Z.; Livolsi, V.; Carrasco, N. Rapid communication: Predominant intracellular overexpression of the Na⁺/I⁻ symporter (NIS) in a large sampling of thyroid cancer cases. *J. Clin. Endocrinol. Metab.* **2001**, *86*, 2697–2700.
153. Luster, M.; Clarke, S.E.; Dietlein, M.; Lassmann, M.; Lind, P.; Oyen, W.J.; Tennvall, J.; Bombardieri, E. Guidelines for radioiodine therapy of differentiated thyroid cancer. *Eur. J. Nucl. Med. Mol. Imaging* **2008**, *35*, 1941–1959.
154. Wapnir, I.L.; van de Rijn, M.; Nowels, K.; Amenta, P.S.; Walton, K.; Montgomery, K.; Greco, R.S.; Dohan, O.; Carrasco, N. Immunohistochemical profile of the sodium/iodide symporter in thyroid, breast, and other carcinomas using high density tissue microarrays and conventional sections. *J. Clin. Endocrinol. Metab.* **2003**, *88*, 1880–1888.
155. Chung, J.K. Sodium iodide symporter: Its role in nuclear medicine. *J. Nucl. Med.* **2002**, *43*, 1188–1200.
156. Klein, H.A.; DiSibio, K.J.; Sims, D.; Singleton, H.C.; Worthy, L.J. I-123 whole body scanning: Case report and discussion. *Clin. Nucl. Med.* **2005**, *30*, 312–316.
157. Gerard, S.K.; Cavalieri, R.R. I-123 diagnostic thyroid tumor whole-body scanning with imaging at 6, 24, and 48 hours. *Clin. Nucl. Med.* **2002**, *27*, 1–8.
158. Mandel, S.J.; Shankar, L.K.; Benard, F.; Yamamoto, A.; Alavi, A. Superiority of iodine-123 compared with iodine-131 scanning for thyroid remnants in patients with differentiated thyroid cancer. *Clin. Nucl. Med.* **2001**, *26*, 6–9.
159. Cancroft, E.T.; Goldsmith, S.J. ^{99m}Tc-pertechnetate scintigraphy as an aid in the diagnosis of breast masses. *Radiology* **1973**, *106*, 441–444.
160. Joseph, J.K.; Patel, R.B.; Damle, A.A.; Nair, N.; Badwe, R.A.; Basu, S. Functional radionuclide imaging, *in-vitro* radioiodine uptake estimation and RT-PCR in the evaluation of sodium iodide symporter (NIS) expression and functionality in breast cancer: A pilot study. *Indian J. Surg. Oncol.* **2013**, *4*, 80–91.

161. Pinto, J.T.; Suffoletto, B.P.; Berzin, T.M.; Qiao, C.H.; Lin, S.; Tong, W.P.; May, F.; Mukherjee, B.; Heston, W.D. Prostate-specific membrane antigen: A novel folate hydrolase in human prostatic carcinoma cells. *Clin. Cancer Res.* **1996**, *2*, 1445–1451.
162. Silver, D.A.; Pellicer, I.; Fair, W.R.; Heston, W.D.; Cordon-Cardo, C. Prostate-specific membrane antigen expression in normal and malignant human tissues. *Clin. Cancer Res.* **1997**, *3*, 81–85.
163. Wright, G.L., Jr.; Haley, C.; Beckett, M.L.; Schellhammer, P.F. Expression of prostate-specific membrane antigen in normal, benign, and malignant prostate tissues. *Urol. Oncol.* **1995**, *1*, 18–28.
164. Mhawech-Fauceglia, P.; Zhang, S.; Terracciano, L.; Sauter, G.; Chadhuri, A.; Herrmann, F.R.; Penetrante, R. Prostate-specific membrane antigen (PSMA) protein expression in normal and neoplastic tissues and its sensitivity and specificity in prostate adenocarcinoma: An immunohistochemical study using multiple tumour tissue microarray technique. *Histopathology* **2007**, *50*, 472–483.
165. Israeli, R.S.; Powell, C.T.; Corr, J.G.; Fair, W.R.; Heston, W.D. Expression of the prostate-specific membrane antigen. *Cancer Res.* **1994**, *54*, 1807–1811.
166. Chang, S.S.; Reuter, V.E.; Heston, W.D.; Hutchinson, B.; Grauer, L.S.; Gaudin, P.B. Short term neoadjuvant androgen deprivation therapy does not affect prostate specific membrane antigen expression in prostate tissues. *Cancer* **2000**, *88*, 407–415.
167. Wernicke, A.G.; Edgar, M.A.; Lavi, E.; Liu, H.; Salerno, P.; Bander, N.H.; Gutin, P.H. Prostate-specific membrane antigen as a potential novel vascular target for treatment of glioblastoma multiforme. *Arch. Pathol. Lab. Med.* **2011**, *135*, 1486–1489.
168. Haffner, M.C.; Kronberger, I.E.; Ross, J.S.; Sheehan, C.E.; Zitt, M.; Muhlmann, G.; Ofner, D.; Zelger, B.; Ensinger, C.; Yang, X.J.; *et al.* Prostate-specific membrane antigen expression in the neovasculature of gastric and colorectal cancers. *Hum. Pathol.* **2009**, *40*, 1754–1761.
169. Rajasekaran, A.K.; Anilkumar, G.; Christiansen, J.J. Is prostate-specific membrane antigen a multifunctional protein? *Am. J. Physiol. Cell. Physiol.* **2005**, *288*, C975–C981.
170. Rajasekaran, S.A.; Anilkumar, G.; Oshima, E.; Bowie, J.U.; Liu, H.; Heston, W.; Bander, N.H.; Rajasekaran, A.K. A novel cytoplasmic tail MXXXL motif mediates the internalization of prostate-specific membrane antigen. *Mol. Biol. Cell.* **2003**, *14*, 4835–4845.
171. Eder, M.; Eisenhut, M.; Babich, J.; Haberkorn, U. PSMA as a target for radiolabelled small molecules. *Eur. J. Nucl. Med. Mol. Imaging* **2013**, *40*, 819–823.
172. Murphy, G.P.; Elgamal, A.A.; Su, S.L.; Bostwick, D.G.; Holmes, E.H. Current evaluation of the tissue localization and diagnostic utility of prostate specific membrane antigen. *Cancer* **1998**, *83*, 2259–2269.
173. Troyer, J.K.; Beckett, M.L.; Wright, G.L., Jr. Detection and characterization of the prostate-specific membrane antigen (PSMA) in tissue extracts and body fluids. *Int. J. Cancer* **1995**, *62*, 552–558.
174. Luthi-Carter, R.; Barczak, A.K.; Speno, H.; Coyle, J.T. Molecular characterization of human brain N-acetylated α -linked acidic dipeptidase (NAALADase). *J. Pharmacol. Exp. Ther.* **1998**, *286*, 1020–1025.
175. Tiffany, C.W.; Lapidus, R.G.; Merion, A.; Calvin, D.C.; Slusher, B.S. Characterization of the enzymatic activity of PSM: Comparison with brain NAALADase. *Prostate* **1999**, *39*, 28–35.

176. Tang, H.; Brown, M.; Ye, Y.; Huang, G.; Zhang, Y.; Wang, Y.; Zhai, H.; Chen, X.; Shen, T.Y.; Tenniswood, M. Prostate targeting ligands based on *N*-acetylated α -linked acidic dipeptidase. *Biochem. Biophys. Res. Commun.* **2003**, *307*, 8–14.
177. Oliver, A.J.; Wiest, O.; Helquist, P.; Miller, M.J.; Tenniswood, M. Conformational and SAR analysis of NAALADase and PSMA inhibitors. *Bioorg. Med. Chem.* **2003**, *11*, 4455–4461.
178. Eder, M.; Neels, O.; Muller, M.; Bauder-Wust, U.; Remde, Y.; Schafer, M.; Hennrich, U.; Eisenhut, M.; Afshar-Oromieh, A.; Haberkorn, U.; *et al.* Novel preclinical and radiopharmaceutical aspects of [^{68}Ga]Ga-PSMA-HBED-CC: A new PET tracer for imaging of prostate cancer. *Pharmaceuticals (Basel)* **2014**, *7*, 779–796.
179. Eder, M.; Wangler, B.; Knackmuss, S.; LeGall, F.; Little, M.; Haberkorn, U.; Mier, W.; Eisenhut, M. Tetrafluorophenolate of HBED-CC: A versatile conjugation agent for ^{68}Ga -labeled small recombinant antibodies. *Eur. J. Nucl. Med. Mol. Imaging* **2008**, *35*, 1878–1886.
180. Eder, M.; Schafer, M.; Bauder-Wust, U.; Hull, W.E.; Wangler, C.; Mier, W.; Haberkorn, U.; Eisenhut, M. ^{68}Ga -complex lipophilicity and the targeting property of a urea-based PSMA inhibitor for PET imaging. *Bioconjug. Chem.* **2012**, *23*, 688–697.
181. Flohr, T. Messprinzip, Bildrekonstruktion, Gerätetyp und Aufnahmetechniken. In *Wie funktioniert CT?* Alkadhi, H., Ed.; Springer-Verlag Berlin Heidelberg: New York, NY, USA, 2011. (In German)
182. Zhang, B.C.; Hou, L.; Lv, B.; Xu, Y.W. Post-marketing surveillance study with iodixanol in 20,185 Chinese patients from routine clinical practices. *Br. J. Radiol.* **2014**, *87*, 20130325.
183. Hasebroock, K.M.; Serkova, N.J. Toxicity of MRI and CT contrast agents. *Expert Opin. Drug Metab. Toxicol.* **2009**, *5*, 403–416.
184. Kuchmiy, A.A.; Efimov, G.A.; Nedospasov, S.A. Methods for *in vivo* molecular imaging. *Biochemistry (Moscow)* **2012**, *77*, 1339–1353.
185. Histed, S.N.; Lindenberg, M.L.; Mena, E.; Turkbey, B.; Choyke, P.L.; Kurdziel, K.A. Review of functional/anatomical imaging in oncology. *Nucl. Med. Commun.* **2012**, *33*, 349–361.
186. Lukaski, H.C. Methods for the assessment of human body composition: Traditional and new. *Am. J. Clin. Nutr.* **1987**, *46*, 537–556.
187. Hansen, G.; Crooks, L.E.; Davis, P.; de Groot, J.; Herfkens, R.; Margulis, A.R.; Gooding, C.; Kaufman, L.; Hoenninger, J.; Arakawa, M.; *et al.* *In vivo* imaging of the rat anatomy with nuclear magnetic resonance. *Radiology* **1980**, *136*, 695–700.
188. Caravan, P.; Ellison, J.J.; McMurry, T.J.; Lauffer, R.B. Gadolinium(III) chelates as MRI contrast agents: Structure, dynamics, and applications. *Chem. Rev.* **1999**, *99*, 2293–2352.
189. Lee, S.H.; Kim, B.H.; Na, H.B.; Hyeon, T. Paramagnetic inorganic nanoparticles as T1 MRI contrast agents. *Wiley Interdiscip. Rev. Nanomed. Nanobiotechnol.* **2014**, *6*, 196–209.
190. Na, H.B.; Song, I.C.; Hyeon, T. Inorganic nanoparticles for MRI contrast agents. *Adv. Mater.* **2009**, *21*, 2133–2148.
191. Bar-Shalom, R.; Valdivia, A.Y.; Blafox, M.D. PET imaging in oncology. *Semin. Nucl. Med.* **2000**, *30*, 150–185.
192. Moses, W.W. Recent advances and future advances in time-of-flight PET. *Nucl. Instrum. Methods Phys. Res. A* **2007**, *580*, 919–924.
193. Yankeelov, T.E.; Abramson, R.G.; Quarles, C.C. Quantitative multimodality imaging in cancer research and therapy. *Nat. Rev. Clin. Oncol.* **2014**, *11*, 670–680.

194. Kauhanen, S.P.; Komar, G.; Seppanen, M.P.; Dean, K.I.; Minn, H.R.; Kajander, S.A.; Rinta-Kiikka, I.; Alanen, K.; Borra, R.J.; Puolakkainen, P.A.; *et al.* A prospective diagnostic accuracy study of 18F-fluorodeoxyglucose positron emission tomography/computed tomography, multidetector row computed tomography, and magnetic resonance imaging in primary diagnosis and staging of pancreatic cancer. *Ann. Surg.* **2009**, *250*, 957–963.
195. Rosenthal, M.S.; Cullom, J.; Hawkins, W.; Moore, S.C.; Tsui, B.M.; Yester, M. Quantitative SPECT imaging: A review and recommendations by the Focus Committee of the Society of Nuclear Medicine Computer and Instrumentation Council. *J. Nucl. Med.* **1995**, *36*, 1489–1513.
196. Alirezapour, B.; Jalilian, A.R.; Bolourinovin, F.; Moradkhani, S. Production and quality control of [(67)Ga]-DOTA-trastuzumab for radioimmunoscintigraphy. *Iran. J. Pharm. Res.* **2013**, *12*, 355–366.
197. Pentlow, K.S.; Finn, R.D.; Larson, S.M.; Erdi, Y.E.; Beattie, B.J.; Humm, J.L. Quantitative imaging of yttrium-86 with PET. The occurrence and correction of anomalous apparent activity in high density regions. *Clin. Positron Imaging* **2000**, *3*, 85–90.
198. Forrer, F.; Valkema, R.; Kwekkeboom, D.J.; de Jong, M.; Krenning, E.P. Neuroendocrine tumors. Peptide receptor radionuclide therapy. *Best Pract. Res. Clin. Endocrinol. Metab.* **2007**, *21*, 111–129.
199. Khalil, M.M.; Tremoleda, J.L.; Bayomy, T.B.; Gsell, W. Molecular SPECT imaging: An overview. *Int. J. Mol. Imaging* **2011**, *2011*, 796025.
200. Ohya, S.; Tamura, T. Nuclear Data: I-123. Available online: http://crete.homeip.net/show_nuclide/530123/ (accessed on 26 February 2015).
201. NCHPS. Nuclide Safety Data Sheet Iodine-131. Available online: <http://hpschapters.org/northcarolina/NSDS/131IPDF.pdf> (accessed on 23 November 2014).
202. McKillop, J.H. Thallium 201 scintigraphy. *West. J. Med.* **1980**, *133*, 26–43.

© 2015 by the authors; licensee MDPI, Basel, Switzerland. This article is an open access article distributed under the terms and conditions of the Creative Commons Attribution license (<http://creativecommons.org/licenses/by/4.0/>).